Revision # 2 – January 31st, 2014

Determination of the concentration of asbestos minerals in highly contaminated mine tailings. The example of the abandoned mine waste of Crètaz and Èmarese (Valle d'Aosta, Italy).

ALESSANDRO F. GUALTIERI,[1,*] SIMONE POLLASTRI,[1] NICOLA BURSI GANDOLFI,[1] FRANCESCO RONCHETTI,[1] CARLO ALBONICO,[2] ALESSANDRO CAVALLO,[3] GIOVANNA ZANETTI,[4] PAOLA MARINI,[4] AND ORIETTA SALA[5]

[1]Dipartimento di Scienze Chimiche e Geologiche, Università di Modena e Reggio Emilia, I-41121 Modena, Italy

[2]A.R.P.A. Valle d'Aosta, I-11020 Saint Christophe Aosta,Italy

[3]Dipartimento di Scienze dell'ambiente e del territorio e di Scienze della terra, Università di Milano-Bicocca, I-20126 Milano, Italy

[4]Dipartimento di Ingegneria delle Materie Prime DIATI - Politecnico di Torino, I-10129 Torino, Italy

[5]A.R.P.A. Emilia Romagna, Sezione Provinciale di Reggio Emilia I-42122, Reggio Emilia, Italy

Submitted to **The American Mineralogist**

*Corresponding author.

Phone: +39 059 2055810; Fax: +39 059 2055887

E-mail address: alessandro.gualtieri@unimore.it

Always consult and cite the final, published document. See http://www.minsocam.org or GeoscienceWorld

ABSTRACT

For the first time, this work reports concentration maps of asbestos minerals in contaminated mine tailings drawn using the results of Rietveld quantitative phase analysis (QPA). The investigates sites are located in the Valle d'Aosta region (Italy): Crètaz, the most important Italian magnetite mine, active until 1979 and Emarèse, one the most important chrysotile asbestos mines in Italy, active until 1968. The results of the study permit to draw the spatial distribution of the asbestos (chrysotile and tremolite in this specific case) concentration, useful to plan reclamation of the sites, with priority given to the areas with the highest asbestos concentration. Because of the complexity of the mineral assemblage which includes, among the others, antigorite, chlorite, talc, and tremolite, the concentration of chrysotile was cross-checked using different experimental techniques such as X-Ray powder diffraction (XRPD), Fourier Transform Infra-Red (FTIR) spectroscopy, scanning electron microscopy (SEM), Polarized light Optical Microscopy (PCOM), and differential thermal analysis (DTA). The accuracy of the results was validated by analyzing standard samples with known concentrations of chrysotile and tremolite. The comparison allowed to point out the advantages and disadvantages of each experimental method.

At Crètaz, chrysotile ranges from 4.4 to 22.8 wt% and tremolite from 1.0 to 10.3 wt% whereas at Emarèse the concentration of chrysotile varies from 3.3 to 39.5 wt% and tremolite from 5.9 to 12.4 wt%. Antigorite and chlorite are the major accompanying phases with variable amounts of other accessory minerals including magnetite, carbonates, talc, olivine, pyroxene, talc, and brucite. The results of our study are of key importance for the local environmental policies as the knowledge of the spatial

Always consult and cite the final, published document. See http://www.minsocam.org or GeoscienceWorld

distribution of the asbestos concentration allows to plan a detailed reclamation agenda of the contaminated sites. The spots with the highest surface contamination of both chrysotile and tremolite were identified and classified as priority area in the reclamation plan.

Keywords: Chrysotile, tremolite, serpentine, mine tailings, quantitative determination

INTRODUCTION

Commercial asbestos minerals are classified into two groups: serpentine and amphibole asbestos, both sharing the same fibrous-asbestiform crystal habit but different structural arrangements at the molecular scale (Bailey 1988). The fibrous-asbestiform variety of serpentine is chrysotile (*white asbestos*) with ideal chemical formula $Mg_3(OH)_4Si_2O_5$. The amphibole asbestos family includes five minerals: actinolite, amosite (fibrous variety of grunerite, *brown asbestos*), anthophyllite, crocidolite (fibrous variety of riebeckite, *blue asbestos*), and tremolite. Amphiboles' have general formula $AB_2C_5T_8O_{22}W_2$ with A = , Ca, K, Li, Na; B = Ca, Fe^{2+}, Li, Mg, Mn^{2+}, Na; C = Fe^{2+}, Fe^{3+}, Li, Mg, Mn^{2+}, Mn^{3+}, Ti^{4+}; T = Al, Si, Ti^{4+}; W = Cl, F, O^{2-}, (OH). The ideal (approximated) formulas of the five asbestos species are: actinolite A = , B = Ca, C = (Fe^{2+}, Mg), T = Si; W = (OH); amosite A = , B = C = Fe^{2+}, T = Si; W = (OH); anthophyllite A = , B = C = Mg, T = Si; W = (OH); crocidolite A = , B = Na, C = (Fe^{2+}, Fe^{3+}, Mg), T = Si; W = (OH); tremolite A = , B = Ca, C = Mg, T = Si; W = (OH).

The six asbestos minerals exhibit outstanding chemical-physical and technological properties exploited for various industrial applications. Chrysotile has been the most commonly used form of asbestos. Regrettably, the unique fibrous-asbestiform crystal

Always consult and cite the final, published document. See http://www.minsocam.org or GeoscienceWorld

habit and surface activity, responsible for the excellent technological properties, also seem to be the cause of asbestos minerals' potential health hazard. The history of the epidemiological reports of asbestos related diseases is well described in Skinner et al. (1988). Although many epidemiological studies provided evidence that amphibole asbestos minerals are more hazardous than chrysotile (Hodgson and Darnton 2000), all six asbestos mineral species are assumed to be harmful to human health. Exposure through inhalation of asbestos minerals may provoke lung diseases (Skinner et al. 1988; Dilek and Newcomb 2003) and during the 1980s, asbestos minerals were declared proven human carcinogens by the US Environmental Protection Agency, the International Agency for Research on cancer (IARC) of the World Health Organization and the National Toxicology Program (Nicholson 1986; IARC 1977; Collegium Ramazzini 2010). Later, many countries worldwide banned or restricted the use of asbestos containing materials (ACMs). In the countries where asbestos minerals are banned, ACMs have been progressively removed from the environment to minimize exposure of the population (Gualtieri 2012). Despite the huge efforts to entirely remove asbestos from the living environment, some issues are still matter of concern. One of these regards the correct evaluation of the health hazard associated with abandoned asbestos mines (especially dumps and tailings) and natural occurring asbestos (NOA). Mining of asbestos and asbestos associated minerals (e.g., iron oxides) generated vast amounts of residue material, chemically not very different from the original rock (Meyer 1980). An important difference is the fineness of the residue material composing the dumps, making it more prone to weathering or erosion by wind, with subsequent release of fibers in air or in the percolating surface hydrological system. With this premise, Viti et al. (2011)

Always consult and cite the final, published document. See http://www.minsocam.org or GeoscienceWorld

suggested that the correct evaluation of the hazard associated with serpentinite outcrops (and asbestos containing mine tailings) would require a careful geo-statistical and geo-mechanical investigation of the fracturing/vein system, followed by careful qualitative and quantitative determinations. Unfortunately, the accomplishment of accurate and precise quantitative figures of the actual asbestos minerals content is made difficult by two major factors: (1) asbestos bearing serpentinite textures typically consist of fine-to-ultrafine intergrowths of fibrous and non-fibrous minerals, often difficult to identify by conventional methods, such as X-ray diffraction or microanalytical approaches. To this aim, DTA seems to be an effective and promising tool of analysis although only a case study has been reported so far (Viti et al. 2011) and further experimental evidence is needed; (2) asbestos and asbestos containing mine dumps and tailings invariably contain high concentrations of asbestos minerals (generally higher than 1wt%). In countries like Italy, regulated experimental techniques for massive materials (X-Ray Powder Diffraction - XRPD, Fourier Transform Infra-red spectroscopy - FTIR, Scanning Electron Microscopy - SEM, and Phase Contrast Optical Microscopy - PCOM) are applied to determine whether asbestos concentration is higher than 0.1 wt% (Italian D.Lgs 10/03/2010 nr. 205 All. D). On the same line, Airborne Toxic Control Measure (ATCM) restricted in the USA the use of serpentine and ultramafic rock aggregates for surface applications to materials containing less than 0.25 wt% asbestos determined according to the Californian Air Resources Board method (CARB method 435, 1991). This scenario reveals that accuracy of these quantitative methods have not been tested for highly contaminated massive materials.

This work was prompted by the actual need to map the concentration of asbestos

Always consult and cite the final, published document. See http://www.minsocam.org or GeoscienceWorld

minerals in abandoned asbestos or asbestos containing open mines with dumps and tailings possibly containing very high concentrations of asbestos fibers (well above 1 wt%). Because the costly reclamation of these sites usually conflicts with the tight budgets of the regional/national funds allocated to such expense items, a step by step long term plan must be proposed with priority given to the reclamation of the areas with the highest asbestos concentration. Therefore, the knowledge of the spatial distribution of the asbestos concentration in such sites is relevant from an economic standpoint as it may permit to prioritize the most hazardous areas within a long term reclamation plan. For the first time, we report the mapping of the concentration of asbestos minerals (chrysotile and tremolite) in abandoned sites with highly contaminated mine tailings. The sites under investigation are located in the Valle d'Aosta region in Italy: Crètaz is situated near the town of Cogne where the most important Italian magnetite mine was active until 1979; Emarèse was one the most important chrysotile asbestos mines in Italy, now abandoned since 1968.

The determination of the chrysotile concentration was accomplished using all the experimental techniques permitted by current Italian regulations for massive materials XRPD, FTIR, SEM, and PCOM. Quantitative PCOM results were integrated by qualitative observations in polarized light (PLOM) and with chromatic dispersion (CD). Although the Italian D.M. 09/06/1994 suggests the use of SEM when the estimated asbestos concentration is lower than 1wt% and MOCF, XRPD and FTIR when it is higher than 1wt%, there is actually no indications on the upper concentration limits of application of SEM. Hence, the analysis of samples with very high concentration of asbestos offers a proper case study. The accuracy of the results was validated by the

Always consult and cite the final, published document. See http://www.minsocam.org or GeoscienceWorld

analysis of especially prepared standard samples with known concentration of chrysotile and tremolite and cross-checked by the application of the Differential Thermal Analysis (DTA) and the Rietveld methods. The comparison allowed to point out the advantages and disadvantages of each experimental method.

GEOLOGY OF THE INVESTIGATED AREA

The main structural lines of the Aosta valley (Fig. 1) are aligned N-W to S-E. They represent a natural cross-section through the structural units of the Italian Alps where the ancient European and African continental margins are divided by relict portions of the oceanic floor. The margin of the European basement emerges in correspondence to the crystalline massif externally represented by the Monte Bianco (Elvetico - Ultraelvetico Domain) and internally by the Gran San Bernardo – Ruitor, the Monte Rosa and the Gran Paradiso (Pennidico Domain). The ancient portion of the Piedmont ocean (the Piedmont Zone with Calc-schists and Green Stones) occurs in the middle stretch of the Valley, spanning the inner margin of the crystalline massifs. The area of the lowest valley is mainly composed by the Pennidic and Austroalpine domains, characterized by folded structures and marked by metamorphism in association with large thrust of the Piedmont Zone of Calc-schists with Green Stones (ophiolites). The mining area of Cogne is found in that formation and emerges in the localities of Aymavilles, Urtier river, and Grauson river (Elter 1987). The rocks of that unit are known to host mineralizations of Cr, Pt, Ni and Fe and various phases such as asbestos minerals and talc. Iron is mostly hosted in magnetite, one of the main constituents of the serpentinite accessories, with the genesis attributed to the processes of serpentinization (hydrothermal alteration of the original

Always consult and cite the final, published document. See http://www.minsocam.org or GeoscienceWorld

mantle peridotites) which began probably in the oceanic environment and continued during the Alpine orogeny (Dal Piaz 1971). The magnetite mines of Cogne, and in particular the site of Crètaz, are located inside the area of the Piedmont Calc-schists and Green Stones (Diella et al. 1994). The ore mining of Cogne was both underground and open (Di Colbertaldo et. al. 1967) and the iron ore has been industrially exploited from 1900 to 1979.

The asbestos Émarèse mine is located inside the Piedmont Zone with Calc-schists and Greenstones (ophiolites). The metabasites which occur at the Émarèse area are mainly composed of serpentinites locally mineralized to antigorite and chrysotile. The latter sometimes occurs in very long fibers that can reach a length of 1 m. Serpentines are accompanied by carbonates, magnetite and talc. The mining activity regarded an open pit and several wells and tunnels (Cavinato 1964). The Émarèse mine is abandoned since 1968.

EXPERIMENTAL PROCEDURE

Materials sampling and sample preparation

A number of representative samples were collected in the areas of Crètaz and Emarèse. Given the extremely hazardous situation due to the proximity of the contaminated site with the touristic town of Cogne, both surface and core sampling was conducted at Crètaz whereas only surface sampling was conducted at Emarèse. As far as the surface sampling is concerned, the materials were collected under a 25-30 mm thick surface layer of soil manually removed with the aid of a shovel. All the operations were conducted using protective equipments. Samples were collected down to a depth of about

Always consult and cite the final, published document. See http://www.minsocam.org or GeoscienceWorld

185 60 mm with the aid of a manual corer. A representative amount of material, depending on
186 the average grain size, was sampled and manually divided with the aid of a Retsch
187 stainless steel sample splitter (maximum capacity = 16 l; maximum grain size = 50 mm)
188 to obtain about 2 Kg of homogeneous final raw product that was finally stored inside
189 glass bottles and sealed. At Crètaz, core sampling was possible using a rotary core drill
190 with a penetration length of about 20 m. Raw core samples were divided and
191 homogenized using the same procedure described above for surface samples. All the
192 surface and core collection spots for both localities are reported in Figure 1. The figure
193 legend also specifies the sampling mode.
194 In the lab, using protective equipments and under extractor fan, raw samples were
195 quartered to obtained about 50 g of homogeneous representative material and
196 subsequently dried at 105 °C for 2 h. Powders were obtained by mechanical milling using
197 Retsch mm 200 SiC jars, with a capacity of 10 ml each, for 10 min at a speed of 25
198 oscillations/s. Further fine manual powdering was conducted using an agate mortar for 5
199 min.
200 Two standard samples (labeled STD1 and STD2) with known contents of chrysotile
201 and tremolite asbestos and mineralogical composition similar to that of the natural
202 samples were prepared as weighed mixtures of artificial tailings to assess the accuracy of
203 the quantitative determination. The compositions of the standard samples (wt%) were:
204 STD1 (chrysotile 5.11, tremolite 5.11, talc 5.11, clinochlore 5.11, antigorite 8.07, calcite
205 40.86, dolomite 10.2, magnesite 4.09, albite 16.34); STD2 (chrysotile 10.44, tremolite
206 1.04, talc 5.22, clinochlore 5.22, antigorite 16.49, calcite 36.53, dolomite 10.44,
207 magnesite 4.18, albite 10.44). Specimens of the mineral phases talc, clinochlore, calcite,

Always consult and cite the final, published document. See http://www.minsocam.org or GeoscienceWorld

dolomite, magnesite, and albite were taken from the mineral collection of the MUSEO GEMMA 1786, Dipartimento di Scienze Chimiche e Geologiche of the University of Modena e Reggio Emilia (Modena, Italy).

The asbestos samples used to prepare the weighed mixtures of artificial tailings are the NIST chrysotile standard SRM1866a and the NIST tremolite sample SRM 1867a, the highest purity available. Bunches of fibers were ultrasonicated and selected under optical microscope. The antigorite sample is from a pale-green, splintery vein occurring in a massive serpentinite from Elba Island (Italy): sample ATG18 in Viti and Mellini (1996). The sample predominantly consists of antigorite lamellae with an average composition of $Mg_{2.62}Fe^{2+}_{0.16}Fe^{3+}_{0.03}(OH)_4Al_{0.01}Si_2O_5$ (normalized to 2 apfu in the tetrahedral site; Loss of Ignition (L.O.I.) of 11.9 wt%) and super-periodicity of 48.8 Å; interstitial chrysotile occurs among antigorite lamellae. The total chrysotile content is 22.0(9) wt% (Viti et al. 2011). Obviously, the chrysotile content of antigorite was considered during the preparation of the mixture. Sample purity of all the selected specimens was checked by XRPD. Prior to the weighing procedure, all the specimens were dried at 105 °C for 2 h and reduced to powders by manual grinding in an agate mortar using acetone as solvent. After weighing the various components, the coarse powders were homogenized and powdered in an agate mortar for 5 min.

Analytical methods

Sample selection

Two natural samples (C2 and E1) and the two standards STD1 and STD2 were selected for the determination of the concentration of chrysotile and tremolite (when

Always consult and cite the final, published document. See http://www.minsocam.org or GeoscienceWorld

possible) asbestos, following the experimental methods considered in the Italian D.M. 09/06/1994, differential thermal analysis (DTA) and X-ray powder diffraction (XRPD) with the Rietveld method. All the other samples collected during the surface and core sampling at Crètaz and Èmarese were analyzed with the Rietveld method to determine both the concentration of chrysotile and tremolite asbestos.

Optical microscopy

As far as the optical microscopy observations are concerned, prior to the qualitative analysis, the samples underwent a chemical attack using a very diluted HCl solution to remove the carbonate fraction and eventually hydrated carbonate alteration products and release the fibers from the matrix. About 0.2 mg of the powder was then suspended in a drop of acetone on a slide, put in a bottle, and inserted in an ultrasonic bath for 15 min. A liquid of proper refraction index is added to the powder on the slide for the polarized light optical microscopy (PCOM) observations. The following refractive indices were used for the identification of the asbestos fibres in the samples: 1.550 for chrysotile; 1.610-1.615 for tremolite; 1.620 for anthophyllite, and 1.640 for actinolite. The microscopes used for the qualitative observations were a Leica DMLP and Leica DIALUX 20.

The samples for the quantitative analyses were prepared by suspending 0.1 mg of powder in 10 ml of distilled water. The suspension was ultrasonicated for 15 min. The suspension was filtered using a 47 mm cellulose nitrate filter to obtain an homogeneous dispersion. The filter was subsequently diaphanized for the PCOM observation. The observations were performed at 500x over a 1.57 mm^2 area of the membrane (0.5% of the total membrane area of 152 mm^2). Each regulated (length > 5 μm and aspect ratio of 3) fiber of both chrysotile and tremolite asbestos observed on the membrane was reported

Always consult and cite the final, published document. See http://www.minsocam.org or GeoscienceWorld

and summed up to calculate the total volume. Assuming theoretical density values of crysotile and tremolite fibers of 2.6 g/cm^3 and 3.0 g/cm^3, respectively, it was possible to calculate the total weight of both asbestos species counted on the membrane. This value was then rescaled to the entire powdered area of the membrane and therefore to the amount (0.1 mg) of powder on it.

Electron microscopy

The scanning electron microscopy (SEM) determinations were performed following the method described in the Italian legislation (Italian Ministry of Health, 1994), which is very similar to the International Standard Organization (ISO) Method 14966 (ISO, 2002). The fiber-definition criteria are those cited above and are compliant with the ISO 14966 and WHO standard (WHO 1997; ISO 2002). An amount of 10 mg of each powder sample was suspended in 200 ml of deionised and micro-filtered water with 0.1 vol.% surfactant additive (dioctyl sodium sulfoccinate, $C_{20}H_{37}NaO_7S$, CAS nr. 577-11-7), and ultrasonicated to facilitate the particle dispersion. A volume of 3 x 2.5 ml of this suspension was collected at different levels and put into a filtering system, allowing random deposition of the particles on polycarbonate filters (Osmonics 25 mm diameter, 0.6 μm porosity). Filters were dried in an oven (at 55 °C), weighed using a high-precision balance and coated with graphite. The samples were analyzed with a Vega TS Tescan 5163 XM SEM (LAB1, the University of Milan-Bicocca), in combination with an energy-dispersive X-ray spectrometer (EDAX Genesis 400), operating at 20 kV and 200 pA, at a working distance of about 20 mm. For each sample, 1 mm^2 of the filter surface was investigated, working at 2000–6000 magnification. The technique is based on point-counting statistics, reporting the occurrence, number, dimension and chemical

Always consult and cite the final, published document. See http://www.minsocam.org or GeoscienceWorld

277 composition of asbestos fibers in each measured spot. The volume of the single fiber is
278 approximated to that of a cylinder, and the weight is calculated assuming an average
279 density of 2.6 g/cm^3 for chrysotile and 3.0 g/cm^3 for all amphibole species. The fiber-
280 concentration C (in ppm) was then calculated as follows:

281 $$C = [A \bullet (w_c + w_a)/n \bullet a \bullet W] \bullet 10^6$$

282 with A = filter surface (mm^2); w_c = total weight of counted chrysotile fibers (mg); w_a =
283 total weight of counted amphibole fibers (mg); n = number of analyzed spots; a = spot
284 surface (mm^2); W = weight of the sample on the filter (mg).

285 The samples (following the protocol of LAB1) were also prepared separately and
286 analyzed in another laboratory (LAB2, A.R.P.A. Aosta). An amount of 10 mg of each
287 powder was suspended in 200 ml of deionised and micro-filtered water with 0.2 vol.%
288 surfactant additive (sodium lauryl sulfate, $CH_3(CH_2)_{11}OSO_3Na$, CAS nr. 151-21-3), and
289 ultrasonically treated. All the other experimental conditions were identical to those
290 reported above. The instrument used for the observations was a Zeiss EVO MA10 with a
291 LaB6 cathode, in combination with an EDAX system, operating at 20 kV and 200 pA,
292 with 500–16000 magnification, at a working distance of 12 mm.

293 *Infrared spectroscopy*

294 For the Fourier transform Infrared (FTIR) spectroscopy measurements, pellets were
295 prepared using 198 mg of dried KBr powder and 2 mg of dried sample powder, with a
296 final load of 12 t for 12 s. A blank standard sample composed of KBr powder was also
297 prepared. Prior to the analysis, a calibration curve with increasing amounts of chrysotile
298 was prepared using the same experimental conditions to apply the Linear Calibration
299 Curve Method (see a through description of the method applied to FTIR in De Stefano et

Always consult and cite the final, published document. See http://www.minsocam.org or GeoscienceWorld

al. 2012). All the spectra were collected from 4000 to 600 cm^{-1} at 4 cm^{-1} resolution using a Bruker VECTOR 22 spectrometer with a Globar source, aperture 3 mm, 32 scans, velocity 10 kHz, detector DTGS with a window of KBr (8000–400 cm^{-1}), Mertz correction phase, apodization function 3-term Blackman-Harris. Data were collected and analyzed using the Bruker OPUS 6.5 software. The intensity of the absorption band at 3697 cm^{-1}, the stretching vibration of chrysotile non-hydrogen-bonded OH^- (Farmer 1974), was measured and plotted versus the added chrysotile weight percent. It is assumed that the detection limit is 0.01 wt% (Foresti et al. 2003). This procedure is rather straightforward when no interference phases such as serpentine polymorphs and chlorite are present (see for example, Balducci and Valerio 1986). The presence in the investigated samples of the layer silicates antigorite and chlorite, which may overlap their absorption bands to that of chrysotile, requires a careful discrimination to obtain the intensity of the chrysotile band to plot vs. chrysotile concentration. For the investigated samples with unknown concentration of chrysotile, the intensity of the absorption band was measured as closest as possible to the ideal value of 3697 cm^{-1} (Farmer 1974), using the "R" type integration process available in the software (the value of the intensity measured above the base line taken between 3720 e 3661 cm^{-1}). The resulting values were then used to extract the chrysotile concentraion from the calibration curve.

X-ray powder diffraction

The XRPD quantitative analysis of chrysotile asbestos has been long conducted using the external standard method (Klug and Alexander 1974) where the peak intensity/integrated area of the major diffraction peak of an analyte (001 peak for chrysotile) is usually plotted vs. its concentration to build a calibration curve. The

Always consult and cite the final, published document. See http://www.minsocam.org or GeoscienceWorld

concentration of the analyte in an unknown sample requires the determination of the correct unbiased intensity/integrated area of the major diffraction peak. Puledda and Marconi (1990) developed a method used for chrysotile legitimated by the Italian D.M. 09/06/1994 which is based on the use of a silver membrane filter. The method also proposes an appropriate value for the deposition area of the sample on filter, which optimizes the diffraction response of the analyte. To apply the method described above, the powder patterns of the samples C2, E1 and the two standards STD1 and STD2 were collected using a Bragg–Brentano θ-θ diffractometer (PANalytical X'Pert Pro), Cu Kα radiation, 40 kV and 40 mA) equipped with a curved graphite monochromator and a gas proportional detector. The divergence, receiving and anti-scattering slits were of 1°, 0.1 mm, and 1°, respectively. The scans were collected with a step scan of 0.02 °2θ, and 5 s/step in the range 4-64 °2θ. The data analysis was performed using the PANalytical HighScore Plus software version 2.2c.

The mineralogical quantitative phase analyses (QPA) of all the Crètaz and Èmarese samples and the two standard samples STD1 and STD2 using the Rietveld method (Rietveld 1969) were performed through X-ray powder diffraction (XRPD). Data were collected using a Bragg–Brentano θ-2θ diffractometer (Bruker D8 Advance, Cu Kα radiation, 40 kV and 40 mA) equipped with a Göbel mirror on the incident beam and a solid state detector. The width of the divergence, receiving and anti-scattering slits were of 0.6, 0.1, and 0.2 mm, respectively. The scans were collected with a step scan of 0.02 °2θ, and 20 s/step in the range 4-65 °2θ. QPAs were performed following the refinement strategies described in Gualtieri (2000). Refinements were accomplished with the GSAS (Larson and Von Dreele 1999) package and its graphical interface EXPGUI (Toby 2001).

Always consult and cite the final, published document. See http://www.minsocam.org or GeoscienceWorld

Whenever the samples showed the presence of more than the maximum number of 9 phases available to the program, the procedure described by Winbur et al. (2000) was used. Although samples were prepared with the side loading technique to minimize *a priori* preferred orientation of crystallites, residual preferred orientation effects were modelled with the March model (Dollase 1986). The following structural models were used: albite (Downs et al. 1994) and plagioclase (Wenk et al. 1980), antigorite (Uehara 1998), calcite, dolomite, quartz (Le Saoût et al. 2011), chrysotile (Falini et al. 2004), chlinochlore (Zanazzi et al. 2009), illite (Birle 1968), magnetite (Haavik et al. 2000), microcline (Ribbe 1979) and orthoclase (Prince et al. 1973), talc (Perdikatsis and Burzlaff 1981), and tremolite (Ungaretti and Oberti 2000).

Thermal analysis

The collection of the thermal analysis curves thermogravimetry (TG), differential thermogravimetry (DTG), and DTA of the C2, E1, and the two standard samples STD1 and STD2 samples were performed using a simultaneous differential thermal analysis (SDTA) SEIKO SSC/5200 SII. Data were collected in air with a flow rate of 2 μl/min, in the range 20–1000 °C, and heating rate of 10 °C/min. Instrumental precision was checked by repeated collections on reference samples, revealing good reproducibility (instrumental theoretical precision of ±0.5 °C); theoretical weight sensitivity is down to 0.1 μg. The DTA traces of the reference samples are reported in Viti (2010). The DTA peak deconvolution has been performed following the method described in Viti et al. (2011). Fitting of the DTA peaks was performed using the deconvolution process available in PeakFit4 (PeakFit Version 4.12, SPSS Inc., AISN Software). The temperature range selected for data analysis is 550–800 °C, that is the main dehydroxylation range, in

Always consult and cite the final, published document. See http://www.minsocam.org or GeoscienceWorld

the attempt to avoid possible interferences with the 820 °C exothermic signals (Viti 2010). The Loess algorithm was used to smooth the data and to remove local perturbations with a ratio of 5%. After that, baseline subtraction was accomplished by a second derivative test procedure.

Although it is well known that both transmission electron microscopy (TEM) and Raman are powerful diagnostic techniques for the study of asbestos containing materials, the two techniques have not been used in this work where the preference was given to the custom methods specifically developed for the determination of the concentration of asbestos minerals in massive materials.

RESULTS

This section is divided into two parts. The first part summarizes the results of each experimental technique applied to the determination of the chrysotile asbestos content in the natural samples C2 and E1, and the two especially prepared standards STD1 and STD2. The second part describes the results of the quantitative phase analysis of the samples collected at Crètaz and Emarèse sites.

Optical observations

The application of the PCOM technique to the study of our samples was of great help from a qualitative point of view as it easily permitted to identify the nature of fiber bunches thanks to the chromatic dispersion (CD) of the fibers (McCrone 1987; NIOSH 1989; EPA 1993; Moss 1994; Bellopede et al. 2009; Cavariani et al. 2010). Figure 2a,b

Always consult and cite the final, published document. See http://www.minsocam.org or GeoscienceWorld

shows beautiful fiber aggregates of chrysotile and tremolite. From a quantitative standpoint, because the fiber counting is usually conducted at a low magnification (generally from 40 to 500x), only fibers or fiber aggregates of considerable size can be observed and counted, and it is sometimes difficult to distinguish between an asbestos fiber and crystal of different nature with acicular crystal habit (Fig. 2c). As a matter of fact, fibers with diameter smaller than 0.8-1 μm are not visible with optical microscopy at 500x with a resolution power of 0.2 μm (Cavariani et al. 2010).

SEM analyses

The SEM determinations allowed to detect even very small fibers (with a length shorter than 1-2 μm) invisible under optical microscope. We have observed that the sample preparation is crucial and a correct fiber counting is possible only if the stub is not overloaded, that is the case when particle aggregates are formed (see an example in Fig. 3a). Small fibers are frequent in the standard samples STD1 and STD2 which were prepared using dry powders. Figure 3b,c reports selected SEM images of the investigated samples showing the presence of fibers with heterogeneous size of both chrysotile and tremolite asbestos fibers. The use of the EDS spot analysis is essential for the correct identification and counting of the chrysotile and tremolite asbestos fibers (Fig. 3c with the relative EDS analysis in the white box). The use of this technique also permits to detect fiber aggregates with distinctive habit and texture and consequently hard to classify otherwise. One such example is portrayed in Figure 3d where an intergrowth of chrysotile-antigorite aggregate is likely observed. Such aggregates may witness low grade regional progressive metamorphism of serpentinite which involves formation of

Always consult and cite the final, published document. See http://www.minsocam.org or GeoscienceWorld

antigorite at expenses of chrysotile (Mellini et al. 1987). This paragenesis has already been reported for the Val Malenco serpentinites in the Italian Alps where chrysotile has been identified as antigorite precursor (Mellini et al. 1987; Wicks and O'Hanley 1988). Notwithstanding, the study of the serpentinite texture and its origin is out of the aims of this paper and should be accomplished using TEM.

FTIR data

Figure 4 portrays the selected region between 3400 and 3950 cm^{-1} of the FTIR spectra of the four investigated samples, where the absorption bands of chrysotile and interference layer silicates occur. The calculated absorbance of the stretching vibration of chrysotile and the resulting chrysotile content (wt%), using the calibration curve with equation y = 0.78269x with y = absorbance (%) and x = chrysotile weight fraction, are reported in Table 1.

XRPD and the Rietveld method

Because the quantitative analysis of chrysotile asbestos using XRPD with the external standard method (Klug and Alexander 1974) requires the determination of the peak intensity or the integrated area of the major diffraction peak of the (001) peak of chrysotile in the unknown sample, the severe peak overlap due to the interference of both antigorite and chlorite, as observed the investigated samples makes this method impracticable. The application of blind single peak fitting procedures to deconvolute each single contribution resulted in unreliable outcomes. For this reason, the use of this method for the determination of the chrysotile asbestos concentration in these matrices

Always consult and cite the final, published document. See http://www.minsocam.org or GeoscienceWorld

turns out to be unfeasible. On the other hand, if a more robust fitting procedure with independent observations and (crystallographic) constraints is applied, deconvolution of each contribution seemed viable. As a matter of fact, the application of the Rietveld method guarantees both the use of independent observations (it is a full profile fitting procedure where all the peaks of each phase in the system are modeled) and robust crystallographic constraints (symmetry, unit cell, profile coefficients, background and others). Accuracy of estimates for multiple serpentine minerals can be achieved because all independent reflections belonging to the different serpentine polymorphs in the collected range can be fitted during the refinement procedure. To this aim, areas where overlap of the peaks of chrysotile and antigorite is limited, with distinct observations that help constrain refinement of these phases, exists: see for example the major (13 $\bar{1}$) peak of antigorite at 2.52 Å which is well separated from chrysotile reflections ($\bar{2}$ 0 2) and (2 0 2), at 2.45 Å and 2.55 Å, respectively. In addition, the fit of a number of peaks of each phase in the systems makes it possible to correct *a posteriori* any preferred orientation effect, if present, which may bias the major intensities of chrysotile, antigorite and chlorite. The result is a very good fit which allows the calculation of the weight estimates of each phase in the system including chrysotile (see the example of sample E1 in Fig 5).

As far as the four analyzed samples, agreement factors of the Rietveld refinements (Larson and Von Dreele 1999) were in the range: R_{wp} = 9.44-10.33%, R_p = 7.07-8.02%, χ^2 = 2.709-5.397. The Rietveld graphical outputs are shown in Figure 6 and Table 2 reports the agreement factors and quantitative phase composition.

DTA analyses

Always consult and cite the final, published document. See http://www.minsocam.org or GeoscienceWorld

Figure 7a-d shows the DTA endothermic signals of the four investigated samples and standard pure chrysotile, due to serpentine dehydroxylation processes in the range 550–850 °C and relative result of the fitting procedure. DTA signals were fit using two peaks for chrysotile (dehydroxylation I and II, weak and strong, respectively) and one peak for antigorite (I in Viti et al. 2011). Figure 7e shows the DTA trace and result of the fitting procedure for the pure chrysotile sample. Only fits with a regression coefficient $R^2 \geq 0.990$ were considered acceptable. The calculated peak areas were reduced to area ratios (ratio between the calculated area in the unknown and that of the pure chrysotile standard) and plotted in the curve obtained by Viti et al. (2011) for antigorite+chrysotile mixtures with a calculated equation of $y = 0.0108x - 0.016$. The results of the procedure are reported in Table 3.

Mineralogical composition and asbestos concentration of the Crètaz and Emarèse samples

Agreement factors of the Rietveld refinements (Larson and Von Dreele 1999) were in the range $R_{wp} = 6.46\text{-}11.32\%$, $R_p = 4.08\text{-}8.01\%$, $\chi^2 = 3.437–8.639$. As an example, the Rietveld graphical output of sample C5 is reported in Figure 8. It should be noted the low peak to background ratio observed in a few samples was due to the fluorescent scattering induced by the large iron content (large magnetite amounts) which excites the copper atoms of the anticathode. Table 4 reports all the quantitative phase compositions of the investigated samples. Because of the low content of magnetite determined in the investigated samples, the microabsorption effects are presumably negligible and no Brindley (1945) correction was applied during the refinement procedure.

Always consult and cite the final, published document. See http://www.minsocam.org or GeoscienceWorld

DISCUSSION

Accuracy of the results from the various experimental techniques

The accuracy of the concentration figures of chrysotile asbestos in the abandoned sites of Crètaz and Emarèse was assessed for two selected samples C2 and E1 and the two especially prepared standards STD1 and STD2, with known asbestos concentration, using the experimental techniques permitted by the current Italian regulation for massive materials (XRPD, FTIR, SEM, and PCOM), the Rietveld method and DTA. Table 5 summarizes the resulting calculated concentration of chrysotile asbestos in the four samples.

Optical microscopy

Although the application of the PCOM technique was qualitatively very useful, the figures obtained with this technique are underestimated with respect to the values provided by the application of the other experimental methods (Table 5): an estimate of 3.7 wt% was calculated for STD1 sample against an expect value of 5.11 wt% and 1.4 wt% for STD2 sample against an expected value of 10.44 wt%. It is possible that limited resolution power did not allow to reckon and quantify small fibers or fiber aggregates predominantly present in the fine powder standards. Analogous conclusions can be found in the literature for the analysis of both airborne and massive sample. As an example, for airborne asbestos fibers in steam tunnels, Dufresne et al. (2002) reported that concentrations found by the TEM/EDS method were higher than those determined by PCOM, especially when chrysotile fibers were present, probably because the TEM/EDS method has a higher resolution than PCOM. Airborne asbestos fibers were present in all

Always consult and cite the final, published document. See http://www.minsocam.org or GeoscienceWorld

the steam tunnels and were barely detectable by the PCOM technique only. Our work confirms the limits of the optical methods and it is not surprising that in many countries optical microscopy was adopted only for the visual qualitative identification of asbestos fibers (see for example, EPA 1989; OSHA 1994; HSE 1994).

Electron microscopy

The chrysotile concentrations obtained from the SEM LAB1 analyses are fairly more accurate than the figures determined from the optical observations. On the other hand, the concentrations provided by SEM LAB2 evidence disagreement (see Table 5). The values provided by LAB1 laboratory are accurate and in agreement with the expected values: an estimate of 4.6 wt% was calculated for STD1 sample against an expect value of 5.11 wt% and 13.1 wt% for STD2 sample against an expected value of 10.44 wt%. Both calculated weights of natural samples C2 and E1 are also in agreement with the values provided by other methods. The values provided by the SEM LAB2 laboratory are largely underestimated as far as the standards are concerned.

Due to the higher resolution power and larger field depth, SEM allows to detect small fibers invisible using the optical microscope. The standards were prepared using chrysotile powders with fine chrysotile fibers hard to detect with an optical microscope even at 500x but clearly visible at 2000x with an electron microscope. This may explain the underestimation in the chrysotile concentration determined with the PCOM technique. The difference in the performance of the two microscopic techniques in favor of the SEM method have already been reported by Cavariani et al. (2010). Cavallo and Rimoldi (2013) who studied similar matrices (asbestos serpentinite quarries in Valmalenco, Central Alps, Northern Italy) reported that the small thickness of chrysotile

Always consult and cite the final, published document. See http://www.minsocam.org or GeoscienceWorld

530 fibrils produced during quarrying activities, and the abundance of pseudo-fibrous
531 antigorite cleavage fragments proved the SEM-EDS analytical procedure to be the most
532 suitable.

533 Concerning the results provide by LAB2, Davies et al. (1996) have previously
534 reported that the method for quantitative analysis of asbestos with SEM for both airborne
535 and massive samples presents difficulties, primarily because of the complexity in
536 standardizing the many operating parameters that are controlled. Although some modern
537 SEMs are capable of resolving surface features at the angstrom level, there is still much
538 difficulty in obtaining adequate images of unit fibrils. Such images are necessary to
539 perform quantitative analyses. Moreover, even though routine SEM/EDS analysis allows
540 evaluation of sample morphology and provides semi-quantitative chemical data, it does
541 not allow determination of crystal structure like TEM. Although TEM is a very time-
542 consuming method, seldom providing concentrations that can be considered
543 representative of the whole sample, it is well known that its use makes it possible to
544 resolve many of the ambiguities that lead to incorrect fiber concentration (Beaman and
545 File 1976; Cattaneo et al. 2012).

546 The underestimation of the fiber concentration from LAB2 may be explained by
547 sample powder heterogeneity. We have observed ball of thread like aggregates of
548 chrysotile fibers within the powders (see Fig. 3e) of the samples prepared in LAB2
549 determining areas with a great concentration of asbestos fibers and areas with no fibers at
550 all. A possible explanation is the use of the surfactant sodium lauryl sulfate for the
551 preparation of the suspension in place of dioctyl sodium sulfoccinate. Sodium lauryl
552 sulfate rises the pH of aqueous solution to about 9.5 whereas dioctyl sodium sulfoccinate

Always consult and cite the final, published document. See http://www.minsocam.org or GeoscienceWorld

stabilizes pH values of the aqueous solution to about 6.2. In distilled water, the zeta potential of chrysotile displays strongly positive values (about +40 mV) at 6.2 and decreases down to about 20 mV at pH = 9.5 (Light and Wei 1977). The decrease of the zeta potential towards the isoelectric point determines instability of the suspension because the particles with low zeta potential have no force to prevent them coming together and flocculating. Jolicouer et al. (1981) used these principles to retard sedimentation of asbestos fibers in NaCl solutions. Hence, the flocculating chrysotile fibers tend to lump together to form the observed ball of thread like aggregate. On a speculative level, it is not possible to rule out that aggregation also occurs in the dry powders, especially those that have undergone physical long-distance transportation and mechanical shaking. In both situations, fiber segregation may bias the sample homogeneity and the representativeness of the microscopic observation usually performed using a tiny amount of powder.

It was already said that the Italian D.M. 09/06/1994 advises the use of SEM when the estimated asbestos concentration is lower than 1wt% giving no indications on the upper concentration limits of application of the method. The concern about asbestos quantitative determination in the case of massive concentration of fibers is related to difficulties for fiber identification and counting due to severe fiber overlap, aggregation and stratification. The results of this study point out that SEM method, if a careful sample preparation, dispersion and representativeness are obtained, can be used even for the quantitative determination of chrysotile asbestos in massive materials with concentrations much larger than 1 wt% with a fairly good accuracy.

Infrared spectroscopy

Always consult and cite the final, published document. See http://www.minsocam.org or GeoscienceWorld

There are many examples of application of FTIR for the quantitative determination of chrysotile asbestos in bulk materials (see for example, Balducci and Valerio 1986; Massola 1997) although some criticism still exists. According to Davies et al. (1996), FTIR is not a sensitive method for quantifying asbestos in loose aggregates and does not produce useful results when multi-component mixtures are analyzed. Oppositely, a positive report is provided by Foresti et al. (2003) who described the application of the FTIR Linear Calibration Curve method for the determination of low levels (0.01–1 wt%) of free fibers of chrysotile in contaminated clayey, sandy and sandy-organic soils. The detection limit of 0.01 wt% was reached with an enrichment of free fibers of chrysotile in the samples using a standard laboratory elutriator for sedimentation analysis. The linearity of the calibration curves obtained for samples having different soil matrices, indicates that the matrix effects can be accounted for. Recently, De Stefano et al. (2012) compared the accuracy and precision of the Linear Calibration Curve Method and the Method of Addition for the FTIR quantitative determination of asbestos bulk matrices and found that, providing careful samples preparation, both techniques quantify the asbestos content at the level of 1-2 wt% with good precision. The results provided in this study are very important as this is one of the few examples of application of the FTIR quantitative method to complex serpentinite samples.

The figures obtained with this method seem rather accurate and in agreement with the values provided by the application of the other experimental methods (Table 5): an estimate of 4.9(2) wt% was calculated for STD1 sample against an expect value of 5.11 wt% and 13.8(2) wt% for STD2 sample against an expected value of 10.44 wt%. Both calculated weights of sample STD2 and E1 (32.9 wt% vs. 25.3 wt% from the Rietveld

Always consult and cite the final, published document. See http://www.minsocam.org or GeoscienceWorld

599 method and 27.5 wt% from the SEM analysis) are apparently overestimated. This
600 discrepancy may be possibly due to: (i) interference of antigorite and chlorite present in
601 the investigated samples with a severe overlap of their absorption bands to that of
602 chrysotile; (ii) deviation of the linearity of the curve intensity of the chrysotile absorption
603 band vs. concentration for large chrysotile contents. The breaking of the linearity
604 assumption has been already observed by De Stefano et al. (2012). They observed that in
605 the case of chrysotile, the peak intensity is a quadratic-like function of the concentration
606 in the extended concentration range.

607 *X-ray powder diffraction*

608 In this work it was found that the XRPD external standard method (Klug and
609 Alexander 1974) is unsuitable for such complex matrices as the observation (e.g., the
610 (001) peak of chrysotile) overlaps to the major peaks of both antigorite (001) and chlorite
611 (002) present in the samples (see sample E1 in Fig. 5), resulting in biased estimates of the
612 integrated area using the single peak fitting deconvolution. The limits of the single peak
613 method for such complex matrices were obvious to Giacomini et al. (2010) who obtained
614 only qualitative estimates of the relative abundance of serpentine polymorphs in samples
615 from the metaophiolites of the the Voltri Massif and Sestri–Voltaggio Zone (Liguria, NW
616 Italy), using the internal standard (20 wt% of corundum) technique and the reference
617 intensity ratio (RIR) method (Snyder and Bish 1989). On the same line, only qualitative
618 determination via XRPD methods were reported by Rigopoulos et al. (2010) for
619 asbestiform minerals in basic and ultrabasic rocks from ophiolite suites of central and
620 northern Greece, Beneduce et al. (2012) for the ophiolites of the Pollino National Park
621 (Calabria-Lucania border, southern Italy), and Cavallo and Rimoldi (2013) for

Always consult and cite the final, published document. See http://www.minsocam.org or GeoscienceWorld

serpentinites of the Valmalenco are (Central Alps, Northern Italy). Puledda and Marconi (1990) assessed the validity of the XRPD external standard method with the Ag filter for synthetic mixtures prepared for the determination of chrysotile content in bulk and airborne samples but did not apply it to natural complex samples such as the one investigated here. It is difficult to evaluate the analytical accuracy of the estimates reported by Davis (1990) who used the RIR method to determine the content of asbestos minerals in synthetic multicomponent mixtures prepared samples demonstrate that the lower limit of detection for most asbestos minerals falls in the range 0.5% to 2 wt%.

On the contrary, the figures obtained with the Rietveld method seem accurate (Table 5): an estimate of 5.8(2) wt% was calculated for STD1 sample against an expect value of 5.11 wt% and 11.2(2) wt% for STD2 sample against an expected value of 10.44 wt%. Sample E1 and C2 also contain fairly large amounts of chrysotile asbestos. The results reported here witness that the Rietveld method can be successfully applied for the determination of chrysotile asbestos in these complex multicomponent samples characterized by the presence of two serpentine polymorphs (antigorite and chrysotile) and chlorite. It is not possible to generalize the outcome of this study and assert that the method is accurate even for more complex samples which contain all the serpentine polymorphs including lizardite, although this mineral association is not rare in green stones. Another critical aspect regards the range of applicability of the Rietveld method in terms of chrysotile content. It is well known that chrysotile possesses a cylindrical lattice with layers curled concentrically or spirally, usually around the *x* axis (*clinochrysotile* and *orthochrysotile*) and seldom around the *y* axis (*parachrysotile*), to form a tubular structure (roll) of about 22±27 nm in diameter (Whittaker 1957; Yada 1971). Moreover,

Always consult and cite the final, published document. See http://www.minsocam.org or GeoscienceWorld

the cylindrical lattice also displays extensive structural defectivity (e.g., random shift component along the fiber axis to yield cone lattices). Such structure complexity results in anisotropic broadening effects of the peak profiles in the X-ray powder patterns which can only be properly fit by recursive models such as the one implemented in DIFFaX+ (Leoni et al. 2004) and not simply by Rietveld-based deterministic codes. For this reason, Wilson et al. (2006) developed and alternative approach to determine the chrysotile content in mine tailings at Clinton Creek (Yukon Territory) and Cassiar (British Columbia) using structure-less pattern fitting and with the addition of a known quantity of a well-crystallized material, by considering the serpentine minerals as amorphous phases, and tested the accuracy of the method using synthetic serpentine-rich mine tailings of known composition. Notwithstanding, marked peak profile broadening effects (especially the asymmetric band in the 19-26 °2θ range due to the destructive interference of non-basal diffraction peaks) are obvious when chrysotile fraction is high. Usually, when chrysotile is present in medium-low concentration, the powder pattern generally displays only the major basal (00*l*) peaks of chrysotile and minor non-basal peaks. Thus, peak profile broadening effects are less obvious and may be modeled by empirical Lorentzian profile anisotropic broadening functions such as the one implemented in GSAS (Larson and Von Dreele 1999): $\gamma = Y + Y_e\cos\phi$ with γ = Lorentzian contribution to the pseudo-Voigt profile function; Y = isotropic strain broadening term; Y_e = anisotropic strain broadening term; ϕ = angle which defines the direction of the broadening axis within the crystallographic setting. Wilson et al. (2006) reported chrysotile estimates as high as 90.8 wt%. For those samples resembling monophasic systems, the accuracy of the Rietveld method is expected to be low. On the other hand, for the systems investigated

Always consult and cite the final, published document. See http://www.minsocam.org or GeoscienceWorld

here with chrysotile contents below 40 wt%, the accuracy of the Rietveld method is still expected to hold. As a matter of fact, the refinement of the anisotropic strain broadening term of the Lorentzian part of the pseudo-Voigt function was attempted for chrysotile for samples C2 and E1, setting the broadening direction along the b axis and the stacking fault model but did not significantly changed the final calculated weights.

Thermal analysis

The quantitative concentration of chrysotile in the standard samples using the DTA method, reported in Table 5, are rather accurate: 7.6 wt% was calculated for STD1 sample against an expect value of 5.11 wt% and 12.2 wt% for STD2 sample against an expected value of 10.44 wt%. Although the successful application of the method has already been reported in the literature for simple systems such as pharmaceutical grade talc where the minimum level of detection was 1% by weight of chrysotile asbestos (Shelz 1974) and in cosmetic grade talc/body products where the minimum level of detection was 0.5% by weight of chrysotile asbestos (Luckewicz 1975), only the recent contribution of Viti et al. (2011) reported accurate estimates for complex natural systems such as serpentinites. Hence, the results of this work are a further confirmation of the reliability of this method. The apparently systematic overestimation should be due to the presence of chlorite in the system. As a matter of fact, Viti et al. (2011) reported that the possible occurrence of other minerals does not hamper the attainment of reliable qualitative determinations, with the only exception of chlorite whose typical DTA curve is characterized by an endothermic peak at 600–650 °C (Smykatz-Kloss 1974), and suggested that, prior to DTA data collection, qualitative XRPD should be performed to ascertain the presence and the amount of chlorite. The presence of chlorite was assessed

Always consult and cite the final, published document. See http://www.minsocam.org or GeoscienceWorld

691 in the first instance via XRPD suggesting the addition of a further peak due to chlorite
692 during the process of fit deconvolution. Notwithstanding, it is possible that a systematic
693 correlation occurred for the calculation of the integrated areas and that the resulting
694 integrated area of chrysotile was underestimated in favor of that of chlorite.
695
696 **Crètaz and Emarèse samples**
697 According to the Italian law D.Lgs 12/03/2010 nr. 205 All. D, if the asbestos
698 concentration is higher than 0.1 wt%, a site should be classified as "contaminated by
699 asbestos". Hence, both Crètaz and Emarèse sites should be reclaimed as all the collected
700 samples consistently show asbestos concentration much higher than the imposed limit
701 (Tables 4 and 5).
702 Figure 9a,b reports maps of concentration of chrysotile and tremolite obtained from
703 the Rietveld analysis for the site of Crètaz (Tables 4 and 5). The maps were obtained by
704 geostatistical analysis of the raw data in GIS environment using the software ArcGIS
705 10.1 and the ArcGIS Geostatistical Analyst application. The Inverse Distance Weighting
706 (IDW) model (Shepard 1968) was used for the deterministic interpolation of the data
707 points. For the chrysotile concentration maps, the following parameters were used: first
708 order model (power = 1), maximum neighbors = 10, minimum neighbors = 5, total
709 calculation area = circular with radius of 138 m. For the tremolite concentration maps, the
710 following parameters were used: second order model (power = 2), maximum neighbors =
711 10, minimum neighbors = 5, total calculation area = circular with radius of 200 m.
712 The chrysotile content varies from 4.4 to 22.8 wt%. In all the samples, chrysotile is
713 associated to antigorite (6.3-50.1 wt%), chlorite (clinochlore 4.1-15.2 wt%), muscovite

Always consult and cite the final, published document. See http://www.minsocam.org or GeoscienceWorld

(2.2-15.8 wt%), quartz (1.9-29.1 wt%), and calcite (4.2-27.5 wt%). The mineral assemblage reflects the overall composition of the mine tailings, a mixing of three different rock types all belonging to the Piedmont Zone unit: the antigorite-serpentinites with magnetite formation, the calc-schists s.l. and local quartzites formation, and the exotic continental Permian-mesozoic succession with schists, quartzites, marbles, and limestones. The distinctive minerals of the latter formation are quartz, mica, carbonates calcite and dolomite, plagioclase, K-feldspar and tremolite (1.8-10.3 wt%). Apparently no trends of the chrysotile and tremolite concentration with (horizontal or vertical) space are observed. This random distribution is due to the history of the various deposits emplaced and mixed with other source of rock dumps during the activity of the mine and not to physical factors such as fiber leaching, transport, and re-deposition. The area with the highest surface concentration of asbestos minerals (see Figure 9) should be considered as priority of intervention in the reclamation plan.

Figure 9c, not elaborated with the geostatistical analysis due to the limited number of raw data points, reports the concentration of chrysotile in the site of Emarèse as obtained from the Rietveld analysis (see also Tables 4 and 5). The chrysotile content varies from 3.3 to 39.5 wt% with the concentration linearly decreasing with the distance from the main mining sites. Chrysotile is invariably accompanied by antigorite (3.3-44.7 wt%) and chlorite (clinochlore 12.4-32.6 wt%). On the basis of the mineral assemblage, two groups of rock samples are observed: (i) samples E1-E5 belongs to the antigorite-serpentinites with magnetite formation of the Piedmont Zone. Besides the typical serpentinite phases antigorite, chrysotile and chlorite, magnetite, talc and brucite are found together with the minerals of the original ultramaphic rock forsterite and enstatite. Hematite, calcite and

Always consult and cite the final, published document. See http://www.minsocam.org or GeoscienceWorld

dolomite are likely secondary phases formed after surface alteration in contact with water; (ii) samples E6-E7 are collected from the surface debris and soil composed of a mixing of the former antigorite-serpentinites with magnetite formation and the calc-schists s.l. and local quartzites formation both belonging to the Piedmont Zone unit. The distinctive minerals of the calc-schists s.l.- quartzite formation are quartz, mica, K-feldspar, plagioclase, and tremolite (5.9-12.4 wt%).

The area with the highest surface concentration of chrysotile (see Figure 9c) should also be classified as prioritary in the reclamation plan.

CONCLUDING REMARKS

A map of the concentration of asbestos minerals chrysotile and tremolite in contaminated mine tailings of the Valle d'Aosta region (Northern Italy) was drawn. The results of this study are strategic as the knowledge of the spatial distribution of the asbestos concentration allows to plan reclamation agenda of the sites. The area with the highest surface concentration of both chrysotile and tremolite were identified and classified as priority in the reclamation plan. The results of our study have general implications as the protocol of sampling, data analysis and mapping of the asbestos concentration can be used in any region of the globe where such deposits are found. Besides that, another general implication of our work regards the assessment of the accuracy of the results obtained using state of the art experimental techniques for the determination of the concentration of asbestos in massive materials. Although we focused on the methods recommended by the Italian laws, the Rietveld method and DTA (Viti et al. 2011) were also included so that a comparison among the various methods used

Always consult and cite the final, published document. See http://www.minsocam.org or GeoscienceWorld

760 worldwide was possible. Accurate estimates were obtained using the SEM, FTIR, XRPD
761 Rietveld and DTA methods whereas poor figures were obtained with the optical
762 microscopy. The single peak fitting XRPD method revealed to be unsuitable because of
763 the interference effects of antigorite and chlorite. It should be remarked that the Rietveld
764 method has been successfully applied for the determination of chrysotile concentrations
765 as high as about 40 wt% in these complex serpentinite multi-component samples
766 characterized by the presence of two serpentine polymorphs (antigorite and chrysotile)
767 and chlorite. Further investigations are required to test the accuracy of the method for
768 even more difficult systems which contain all the three serpentine polymorphs, including
769 lizardite. With higher concentrations (>50 wt%?), it is recommended to apply other
770 methods such as the one proposed by Wilson et al. (2006) who determined the chrysotile
771 content in asbestos mine tailings using structure-less pattern fitting and with the addition
772 of a known quantity of a standard material so to be able to consider the serpentine
773 minerals as amorphous phases.
774

775 **Acknowledgments**

776 Thanks are due to the technical staff of the C.I.G.S. Laboratory (The University of
777 Modena and R.E., Modena Italy). Thanks to the staff of the CGT - Centro di Geo
778 Tecnologie) University of Siena, Italy for help with the FTIR analyses. Thanks to A.
779 Facchinetti and A. Zanella (ARPA Valle d'Aosta, Sezione Analisi strutturali e amianto)
780 for their help with the SEM analyses. This manuscript benefited greatly from the accurate
781 revisions of Dr. S.A. Wilson and suggestions of the Associate Editor Prof. M. Gunter.
782

Always consult and cite the final, published document. See http://www.minsocam.org or GeoscienceWorld

REFERENCES CITED

Bailey, K. F. (1988) Hydrous Phyllosilicates (exclusives of micas) Vol. 19. Series editor P. H. Ribbe. Mineralogical Society of America, pp., 518.

Balducci, D. and Valerio, F. (1986) Qualitative and Quantitative Evaluation of Chrysotile and Crocidolite Fibers with IR-Spectroscopy: Application to Asbestos-Cement Products. International Journal of Environmental Analytical Chemistry 27(4), 315-323.

Beaman, D.R. and File, D.M. (1976) Quantitative determination of asbestos fiber concentrations. Analytical Chemistry, 48, 101–110.

Bellopede, R., Clerici, C., Marini, P. and Zanetti, G. (2009) Rocks with Asbestos: Risk Evaluation by Means of an Abrasion Test. American Journal of Environmental Sciences, 5(4), 500-506.

Beneduce, P., Di Leo, P., Ivo Giano, S. and Schiattarella, M. (2012) Quantitative geomorphic analysis of asbestos dispersion and pollution from natural sources: the case-history of the Pollino national park, southern Italy. Geografia fisica e Dinamica del Quaternario (in Italian), 35, 3-12.

Birle, J. D., Gibbs, G. V., Moore, P. B. and Smith, J. V. (1968) Crystal structures of natural olivines. American Mineralogist, 53, 807-824.

Brindley, G. W. (1945) The effect of particle size and microabsorption on diffracted powder line intensities. Philosophical Magazine, 36, 347-369.

CARB Method 435, (1991) Determination of asbestos content of serpentinite aggregate. State of Air Resources Board,California. http://www.arb.ca.gov/testmeth/vol3/M_435.pdf

Always consult and cite the final, published document. See http://www.minsocam.org or GeoscienceWorld

Cattaneo, A., Somigliana, A., Gemmi, M., Bernabeo, F., Savoca, D., Domenico, M. Cavallo, and P.A., Bertazzi (2012) Airborne Concentrations of Chrysotile Asbestos in Serpentine Quarries and Stone Processing Facilities in Valmalenco, Italy. Annals of Occupational Hygiene, 56(6), 671–683.

Cavallo, A. and Rimoldi, B. (2013) Chrysotile asbestos in serpentinite quarries: a case study in Valmalenco, Central Alps, Northern Italy. Environmental Science: Processes & Impacts, in press.

Cavariani, F., Marconi, A. and Sala, O. (2010) Asbestos: sampling, analytical techniques and limit values. Italian Journal of Occupational and Environmental Hygiene, 1(1), 18-28.

Cavinato, A. (1964) I Giacimenti minerari. Torino : UTET, stampa 1964. - XLVII, pp. 686 (in Italian).

Collegium Ramazzini (2010), 'Asbestos is still with us: repeat call for universal ban', *Occupational Med*icine, 60, 584–588.

Dal Piaz, G.V. (1971) Alcune considerazioni sulla genesi delle ofioliti piemontesi e dei giacimenti ad esse associati. Bollettino Associazione Mineralogica Subalpina, Torino, 8: 365-388 (in Italian).

Davies, L.S.T., Wetherill, G.Z., McIntosh, C., McGonagle, C., and Addison, J. (1996) Development and validation of an analytical method to determine the amount of asbestos in soils and loose aggregates. HSE Contract research Report No. 83/1996, pp. 69.

Davis, B.L. (1990) Quantitative Analysis of Asbestos Minerals by the Reference Intensity X-Ray Diffraction Procedure. American Industrial Hygiene Association Journal,

Always consult and cite the final, published document. See http://www.minsocam.org or GeoscienceWorld

51(6), 297-303.

De Stefano, L., Cioffi, R. and Colangelo, F. (2012) Comparison between Two FTIR Spectroscopy Analytical Procedures for Micrograms Determination of Asbestos Species in Bulk Materials. American Journal of Analytical Chemistry, 3, 1-5.

Di Colbertaldo, D., Di Furia, E. and Rossi, F. (1967) Il giacimento a magnetite di Cogne in Val d'Aosta. Rendiconti Istituto Lombardo, 101, 361-394 (in Italian).

Diella, V., Ferrario, A. and Rossetti, P. (1994) The magnetite ore deposits of the southern Aosta Valley: chromitite transformed during an alpine metamorphic event. Ofioliti, 19, 247-256.

Dilek, Y. and Newcomb, S. (Eds.) (2003) Ophiolite concept and the evolution of geological thought (No. 373). Geological society of America, pp. 505.

Dollase, W.A. (1986) Correction of intensities for preferred orientation in powder diffractometry: application of the March model. Journal of Applied Crystallography, 19, 267-272.

Downs, R.T., Hazen, R.M. and Finger, L.W. (1994) The high-pressure crystal chemistry of low albite and the origin of the pressure dependency of Al-Si ordering. American Mineralogist, 79, 1042-1052.

Dufresne, A., Anthes, M., Santos, B. and Infante-Rivard, C. (2002) Airborne Asbestos Fibres in Steam Tunnels: A Qualitative Analysis by PLM and a Quantitative Analysis by PCOM and TEM/EDS. Annals of Occupational Hygiene, 46(1), 125–127.

Elter, G. (1960) La zona pennidica dell'alta e media Valle d'Aosta e le sue unità limitrofe. Memorie Istituto Geologia e Mineralogia Università di Padova (Italy), 22,

Always consult and cite the final, published document. See http://www.minsocam.org or GeoscienceWorld

113 (in Italian).

Environmental Protection Agency (EPA) (1989) Code of Federal Regulations, Pt. 763, Appendix A- Interim method of the determination of asbestos in bulk insulation samples, July 1989.

Environmental Protection Agency (EPA) (1993) Test Method - Method for the determination of asbestos in bulk building materials. EPA/600/R-93/116, July 1993.

Falini, G., Foresti, E., Gazzano, M., Gualtieri, A.F., Leoni, M., Lesci, I.G. and Roveri, N. (2004) Tubular-shaped stoichiometric chrysotile nanocrystals. Chemistry European Journal, 10, 3043–3049.

Farmer, V.C. (1974) The Infrared Spectra of Minerals. The Mineralogical Society, London, U.K, pp. 539.

Foresti, E., Gazzano, M., Gualtieri, A.F., Lesci, I.G., Lunelli, B., Pecchini, G., Renna, E. and Roveri, N. (2003) Determination of low levels of free fibres of chrysotile in contaminated soils by X-ray diffraction and FTIR spectroscopy. Analytical and Bioanalytical Chemistry, 376, 653–658.

Giacomini, F., Boerio, V., Polattini, S., Tiepolo, M., Tribuzio, R. and Zanetti, A. (2010) Evaluating asbestos fibre concentration in metaophiolites: A case study from the Voltri Massif and Sestri-Voltaggio Zone (Liguria, NW Italy). Environmental Earth Sciences, 61, 1621–1639.

Gualtieri, A.F. (2000) Accuracy of XRPD QPA using the combined Rietveld–RIR method. Journal of Applied Crystallography, 33, 267–278.

Always consult and cite the final, published document. See http://www.minsocam.org or GeoscienceWorld

Gualtieri, A. F. (2012) : Mineral fibre-based building materials and their health hazards. Chapter 8 nel volume "Toxicity of Building Materials" (pp. 486), Edited by F. Pacheco-Torgal, S. Jalali and A. Fucic, Woodhead Publishing, 166-195.

Haavik, C., Stølen, S., Fjellvåg, H., Hanfland, M. and Häusermann, D. (2000) Equation of state of magnetite and its high-pressure modification: Thermodynamics of the Fe-O system at high pressure. American Mineralogist, 85(3-4), 514-523.

Hodgson, J. T. and Darnton, A. (2000) The quantitative risks of mesothelioma and lung cancer in relation to asbestos exposure. Annals of Occupational Hygiene, 44 (8), 565-601.

IARC (International Agency for Research on Cancer) (1977) IARC Monographs on the Evaluation of the Carcinogenic Risk of Chemicals to Man: Asbestos. IARC Monographs on the Evaluation of Carcinogenic Risk of Chemicals to Man, 14, 1-106.

ISO (International Standard Organization) (2002) Ambient air determination of numerical concentration of inorganic fibrous particles scanning electron microscopy method 14966. Geneva, Switzerland.

Jolicoeur, C. and Duchesne, D. (1981) Infrared and thermogravimetric studies of the thermal degradation of chrysotile asbestos fibres: evidences for matrix effects. Canadian Journal of Chemistry, 59, 1521–1526.

Klug, H. P. and Alexander, L. E. (1974) X-ray Diffraction. Addision-Wilson Publishing Company Inc, USA, 132 pp. 966.

Larson, A.C. and Von Dreele, R.B. (1999) Generalized Structure Analysis System. Los Alamos National Lab, New Mexico, LAUR 86-748.

Always consult and cite the final, published document. See http://www.minsocam.org or GeoscienceWorld

Leoni, M., Gualtieri, A.F., and Roveri, N. (2004) Simultaneous refinement of structure and microstructure of layered materials. Journal of Applied Crystallography, 37, 166–173.

Le Saoût, G, Kocaba, V. and Scrivener, K. (2011) Application of the Rietveld method to the analysis of anhydrous cement. Cement and Concrete Research, 41, 133-141.

Light, W. G. and Wei, E. T. (1977) Surface charge and hemolytic activity of asbestos. Environmental Research, 13(1), 135-145.

Luckewicz, W. (1975) Differential thermal analysis of Chrysotile asbestos in pure talc and talc containing other minerals. Journal of the Society of Cosmetics Chemistry, 26, 431-437.

Massola, A. (1997) Campionamento e analisi di materiali contenenti amianto. L'amianto: dall'ambiente di lavoro all'ambiente di vita. Nuovi indicatori per futuri effetti a cura di Minoia C., Scansetti G., Piolatto G., Massola A. Laboratorio di Igiene Ambientale e Tossicologia Industriale, Fondazione "S. Maugeri". Clinica del Lavoro e della Riabilitazione, (I.R.C.C.S.). Centro Medico di Pavia. I Documenti. 12 (in Italian).

McCrone, W.C. (1987) Asbestos identification: Chicago, Illinois, McCrone Research Institute, G&C Printers Inc., pp. 199.

Mellini, M., Trommsdorff, V. and Compagnoni, R. (1987) Antigorite polysomatism: Behaviour during progressive metamorphism. Contributions to Mineralogy and Petrology, 97, 147–155.

Meyer, D. R. (1980) Nutritional problems associated with the establishment of vegetation on tailings from an asbestos mine. Environmental Pollution (Series A), 23, 287 – 298

Moss, R.D. (1994) Evaluation of asbestos quantitation methods. Microscope, 42, 7-14.

Always consult and cite the final, published document. See http://www.minsocam.org or GeoscienceWorld

Nicholson W. J. (1986) Airborne asbestos health assessment update. NTIS, SPRINGFIELD, VA(USA).

NIOSH (National Institute of Occupational Safety and Health) (1989) Asbestos (bulk), Method 9002: Microscopy, Stereo and Polarized Light with Dispersion Staining. NIOSH Manual of Analytical Methods, 5/15/89.

OSHA (Occupational Health and Safety Administration) (1994) Occupational Exposure to Asbestos. Federal Register 59, 40964, August 10, 1994.

Perdikatsis, B. and Burzlaff, H.(1981) Strukturverfeinerung am talk $Mg_3[(OH)_2Si_4O_{10}]$. Zeitschrift für Kristallographie, 156(3-4), 177-186.

Prince, E., Donnay, G., Martin, R.F. (1973) Neutron diffraction refinement of an ordered orthoclase structure. American Mineralogist, 58, 500-507.

Puledda, S. and Marconi, A. (1990) Quantitative X-ray diffraction analysis of asbestos by the silver membrane filter method. Application to chrysotile. Am. Ind. Hyg. Assoc. J., 51, 107-114.

Ribbe, P.H. (1979) The structure of a strained intermediate microcline in cryptoperthitic association with twinned plagioclase. American Mineralogist, 64, 402-408.

Rietveld, H.M. (1969) A profile refinement method for nuclear and magnetic structures. J Applied Crystallography, 2, 65–71.

Rigopoulos, I., Tsikouras, B., Pomonis, P., Karipi, S. and Hatzipanagiotou, K. (2010) Quantitative analysis of asbestos fibres in ophiolitic rocks used as aggregates and hazard risk assessment for human health. Bulletin of the Geological Society of Greece, Proceedings of the 12th International Congress, Patras, May, 2010

Always consult and cite the final, published document. See http://www.minsocam.org or GeoscienceWorld

Shelz, J. P. (1974) The detection of chrysotile asbestos at low- levels of talc by differential thermal analysis. Thermochimica Acta, 197-204.

Shepard, D. (1968) A two-dimensional interpolation function for irregularly spaced data. Proceedings of the 1968 ACM National Conference, 517–524.

Skinner, H.C.W., Ross, M. and Frondel, C. (1988) Asbestos and other fibrous materials - mineralogy, crystal chemistry and health effects: New York, Oxford, Oxford University Press, pp. 204.

Smykatz-Kloss, W. (1974) Differential Thermal Analysis. Application and results in mineralogy, Springer-Verlag, Berlin, pp.185.

Snyder, R.L. and Bish, D.L. (1989) Quantitative Analysis, in Bish, D.L. and Post, J.E., eds., Modern Powder Diffraction, Reviews in Mineralogy, v. 20, Washington, D.C., Mineralogical Society of America, 101-144.

Toby, B.H. (2001) EXPGUI, a graphical user interface for GSAS. Journal of Applied Crystallography, 34, 210–213.

Uehara, S. (1998) TEM and XRD study of antigorite superstructures. The Canadian Mineralogist, 36, 1595-1605.

Ungaretti, L. and Oberti, R. (2000) Leverage analysis and structure refinement of minerals. American Mineralogist, 85(3-4), 532-542.

Viti, C. (2010) Serpentine minerals discrimination by thermal analysis. American Mineralogist, 95, 631–638.

Always consult and cite the final, published document. See http://www.minsocam.org or GeoscienceWorld

Viti, C. and Mellini M. (1996) Vein antigorites from Elba Island, Italy. European Journal of Mineralogy, 8, 423–434.

Viti, C., Giacobbe, C. and Gualtieri, A.F. (2011) Quantitative determination of chrysotile in massive serpentinites using DTA: Implications for asbestos determinations. American Mineralogist, 96, 1003–1011.

Wenk, H.R., Joswig ,W., Tagai, T., Korekawa, M. and Smith, B.K. (1980) The average structure of An 62-66 labradorite. American Mineralogist, 65, 81-95.

Wicks, F. J. and O'Hanley, D. S. (1988) : Serpentine minerals; structures and petrology Reviews in Mineralogy and Geochemistry, 19, 91-167.

Winburn, R.S., Grier, D.G., McCarthy, G.J. and Peterson, R.B. (2000) Rietveld quantitative X-ray diffraction analysis of NIST fly ash standard reference materials. Powder Diffraction, 15, 163-172.

Whittaker, E.J.W. (1957) The structure of Chrysotile, V. diffuse reflexions and fibre texture Acta Crystallographica, 10, 149-156.

WHO (World Health Organization) (1997) Determination of airborne fiber number concentrations; a recommended method, by phase contrast microscopy (membrane filter method). Geneva, Switzerland.

Wilson, S. A., Raudsepp, M. and Dipple, G. M. (2006) Verifying and quantifying carbon fixation in minerals from serpentine-rich mine tailings using the Rietveld method with X-ray powder diffraction data. American Mineralogist, 91, 1331–1341.

Yada K. (1971) Study of microstructure of chrysotile asbestos by high-resolution electron microscopy, Acta Crystallographica A, 27(6), 659-664.

Always consult and cite the final, published document. See http://www.minsocam.org or GeoscienceWorld

Zanazzi, P.F., Comodi, P., Nazzareni, S., and Andreozzi, G.B. (2009) Thermal behaviour of chlorite: an *in situ* single-crystal and powder diffraction study. European Journal of Mineralogy, 21(3), 581-589.

Always consult and cite the final, published document. See http://www.minsocam.org or GeoscienceWorld

Figure Captions

FIGURE 1. Sketch map of the geology of Valle d'Aosta (1:1.000.000 scale; Legend: Austroalpine System (1 = Diorite–Kinzigite Zone, 2 = Gneiss Complex, 3 = Eclogitic Micaschist Complex); Piedmont Zone with Calc-schists and Greenstones (4 = Oceanic Metasedimentary overlay, 5 = Metabasites); Pennidic System (6 = Upper Pennidic Zone, 7 = Middle Pennidic Zone, 8 = Outer Pennidic Zone; 9 = Ultra-elvetic System; 10 = Elvetic System) and location of the surface and core collection spots for the two investigated sites: (a) Crètaz with C1-C8 = surface samples, depth 0.25-0.3 m; C9v1 = drill 1, depth 0.7 m; C10v1 = drill 1, depth 7.5 m; C11v1 = drill 1, depth 15 m; C12v1 = drill 1, depth 19.2 m; C13v2 = drill 2, depth 0.5 m; C14v2 = drill 2, depth 11 m; C15v2 = drill 2, depth 22.4 m. (b) Emarèse with E1-E8 = surface samples.

FIGURE 2. Selected PCOM images of the investigated samples (see text for details). Legend: (a) chrysotile at 10x in liquid with refractive index of 1.550; (b) tremolite fibers at 10x in liquid with refractive index of 1.615; (c) non-asbestos acicular-like crystal: diopside at 10x in liquid with refractive index of 1.670.

FIGURE 3. Selected SEM images of the investigated samples (see text for details). Legend: (a) particle and fiber aggregates difficult to detect and count; (b) chrysotile fibers of heterogeneous size; (c) tremolite fibers with the relative EDS point analysis which permits the discrimination from other fibrous phases; (d) example of intergrowth of mixed chrysotile-antigorite aggregate; (e) ball of thread like aggregates of chrysotile fibers within the powders of the samples prepared in LAB2 (see the text for details).

FIGURE 4. The FTIR spectra region between 3400 and 3950 cm^{-1} of the four investigated samples where the absorption bands of chrysotile and interference layer

Always consult and cite the final, published document. See http://www.minsocam.org or GeoscienceWorld

silicates occur. (a) STD1; (b) STD2; (c) C2; (d) E1.

FIGURE 5. Selected low angle region of sample E1 showing severe overlap of the peaks of chrysotile, antigorite and clinochlore and the result of the peak fitting using the Rietveld method.

FIGURE 6. The Rietveld graphical outputs of the samples selected for the accuracy verification. Crosses represent the observed pattern, the thin line represents the calculated pattern and the grey bottom line is the difference line. Markers of all the peaks of the each crystalline phase included in the refinement procedure are also shown in different lines. Legend: (a) STD1, lines of peak markers from the bottom: antigorite, chrysotile, tremolite, talc, clinochlore, calcite, dolomite, magnesite, albite. (b) STD2, lines of peak markers from the bottom: antigorite, chrysotile, tremolite, talc, clinochlore, calcite, dolomite, magnesite, albite; (c) C2, lines of peak markers from the bottom: antigorite, chrysotile, tremolite, muscovite, clinochlore, calcite, quartz, K-feldspar, albite; (d) E1, lines of peak markers from the bottom: antigorite, chrysotile, clinochlore, calcite, magnetite, forsterite, hematite, enstatite, brucite.

FIGURE 7. DTA traces of the four investigated samples and standard pure chrysotile, in the range 550–850 °C (see the text for details) with the result of the deconvolution fitting procedure. Legend: (a) STD1; (b) STD2; (c) C2; (d) E1; (e) pure chrysotile.

FIGURE 8. The Rietveld graphical output of sample C5. Crosses represent the observed pattern, the thin line represents the calculated pattern and the grey bottom line is the difference line. Markers of all the peaks of the each crystalline phase included in the refinement procedure are shown. Legend from the bottom line: antigorite, chrysotile, tremolite, muscovite, clinochlore, calcite, quartz, K-feldspar, dolomite.

Always consult and cite the final, published document. See http://www.minsocam.org or GeoscienceWorld

FIGURE 9. Maps of concentration of chrysotile (a) and tremolite (b) obtained from the Rietveld analysis for the site of Crètaz obtained by geostatistical analysis of the raw data in GIS environment using the software ArcGIS 10.1 and the ArcGIS Geostatistical Analyst application. The raw concentrations of chrysotile for the site of Emarèse are plotted in (c).

Always consult and cite the final, published document. See http://www.minsocam.org or GeoscienceWorld

Tables

TABLE 1. The calculated absorbance (%)of the stretching vibration of chrysotile and the resulting chrysotile content (wt%), using the calibration curve with equation y = 0.78269x with y = absorbance (%) and x = chrysotile weight fraction.

Sample	absorbance (%)	chrysotile content (wt%)	chrysotile content error
STD1	3.856	4.9	0.03
STD2	10.801	13.8	0.02
C2	4.931	6.3	0.02
E1	25.75	32.9	0.02

Always consult and cite the final, published document. See http://www.minsocam.org or GeoscienceWorld

1126 **TABLE 2.** The results of the Rietveld quantitative phase composition. The definition of

1127 the agreement factors is reported in Larson and Von Dreele (1999).

	STD1	STD2	C2	E1
R_{wp} (%)	10.3	9.73	10.33	9.44
R_p (%)	8.02	7.51	7.57	7.07
χ^2	5.40	2.71	5.40	6.32
antigorite	6.9(3)	14.9(3)	3.5(3)	44.7(6)
brucite	-	-	-	0.3(1)
calcite	39.3(2)	36.7(3)	8.0(3)	2.6(2)
chrysotile	5.8(2)	11.2(3)	6.3(4)	25.1(9)
clinochlore	4.6(2)	5.9(3)	7.5(3)	15.8(4)
dolomite	11.9(2)	11.7(2)	-	-
hematite	-	-		1.3(2)
enstatite	-	-		1.2(3)
forsterite	-	-		4.0(6)
K-feldspar	-	-	4.2(3)	-
magnesite	4.3(2)	4.6(2)	-	-
magnetite	-	-	-	5.0(2)
muscovite/Illite	-	-	10.9(5)	-
plagioclase	18.3(2)	10.8(3)	22.4(3)	-
quartz	-	-	32.6(2)	-
talc	3.3(5)	3.2(3)	-	-
tremolite	5.6(3)	1.0(3)	4.6(3)	-
TOT	100	100	100	100

1128

1129

Always consult and cite the final, published document. See http://www.minsocam.org or GeoscienceWorld

TABLE 3. The results of the chrysotile determination using the DTA method (see the text for details).

Sample	Sum of the peak area	Error	r^2	Calculated wt% chrysotile	Area ratio	Error
Pure chrysotile standard	1358	39	0.9909	100	1	n.d.
STD1	89	16	0.9927	7.6	0.06	0.03
STD2	155	8	0.9921	12.2	0.11	0.02
C2	108	3	0.9952	8.9	0.08	0.07
E1	300	26	0.9955	22.2	0.22	0.07

Always consult and cite the final, published document. See http://www.minsocam.org or GeoscienceWorld

TABLE 4. The quantitative phase compositions of the Crètaz and Emarèse samples. The definition of the agreement factors is reported in Larson and Von Dreele (1999).

	C1	C2	C3	C4	C5	C6	C7	C8	C9V1	C10V1	C11V1	C12V1
R_{wp} (%)	7.68	10.33	6.46	8.8	5.64	11.32	7.12	6.98	7.8	7.86	3.29	10.48
R_p (%)	5.58	7.57	4.81	6.22	4.08	8.01	5.51	5.42	5.94	6.02	5.55	7.93
χ^2	5.55	5.40	3.44	6.60	3.87	8.64	2.55	2.96	3.33	3.35	2.64	5.61
antigorite	32.4(8)	3.5(3)	29.5(6)	47.1(6)	39.3(7)	50.1(6)	30.9(5)	23.6(4)	40.4(4)	19.5(7)	14.3(4)	52.4(5)
calcite	20.5(3)	8.0(3)	4.2(2)	9.0(3)	11.5(3)	8.1(3)	12.0(2)	8.0(2)	14.7(2)	27.5(2)	16.6(2)	5.0 (2)
chrysotile	6.2(9)	6.3(4)	4.4(6)	11.4(8)	9.7(8)	11.2(7)	15.8(4)	11.6(4)	11.8(4)	12.1(5)	6.0(3)	22.8(5)
clinochlore	13.4(5)	7.5(3)	10.0(3)	12.0(6)	6.1(5)	11.4(5)	15.2(5)	7.0(3)	10.1(5)	9.4(6)	9.0(3)	7.9(7)
dolomite	4.3(5)	-	-	2.3(5)	2.8(5)	2.2(5)	15.0(3)	-	-	4.6(2)	-	-
K-feldspar	3.5(4)	4.2(3)	1.7(3)	2.9(4)	5.1(4)	2.1(3)	-	-	-	-	-	-
magnetite	-	-	-	-	-	-	4.9(1)	2.5(1)	3.6(2)	4.7(1)	1.3(1)	4.2(2)
muscovite/Illite	9.6(8)	10.9(5)	15.8(5)	8.3(8)	13.1(1)	8.4(7)	2.2(6)	10.3(5)	7.8(6)	9.3(6)	20.4(4)	2.2(7)
plagioclase	-	22.4(3)	3.3(4)	-	-	-	-	6.3(3)	-	-	-	-
quartz	2.0(3)	32.6(2)	28.8(2)	3.8 (4)	5.4(2)	4.1(1)	3.5(2)	17.6(1)	5.6(1)	10.2(2)	29.1(2)	3.4(2)
talc	0.5(2)	-	0.5(2)	-	-	-	0.5(2)	2.8(2)	2.1(2)	2.7(3)	3.3(3)	2.1(3)
tremolite	7.6(6)	4.6(3)	1.8(4)	3.2(5)	7.0(5)	2.4(5)	-	10.3(1)	3.9(5)	-	-	-
TOT	100	100	100	100	100	100	100	100	100	100	100	100

Always consult and cite the final, published document. See http://www.minsocam.org or GeoscienceWorld

	C13V2	C14V2	C15V2	E1	E2	E3	E4	E5	E6	E7	E8
R_{wp} (%)	8.29	8.61	7.6	9.44	10.9	10.44	9.23	10.31	8.36	6.6	6.01
R_p (%)	6.29	6.73	5.77	7.07	8.13	7.64	6.94	7.53	6.26	5.09	4.67
χ^2	3.99	3.54	2.87	6.32	8.68	8.89	6.35	10.41	5.87	3.32	3.20
antigorite	35.4(5)	35.1(4)	6.3(4)	44.7(6)	21.4(5)	13.5(3)	7.1(2)	17.1(3)	3.3(2)	7.7(3)	8.8(3)
brucite	-	-	-	0.3(1)	2.0(3)	1.0(3)	1.1(2)	1.4(3)	-	-	-
calcite	12.0(3)	9.8(2)	5.0(2)	2.6(2)	-	3.5(2)	2.9(2)	4.9(3)	2.0(5)	1.3(2)	-
chrysotile	14.7(5)	21.9(4)	5.2(3)	25.1(9)	39.5(9)	35.0(9)	39.5(8)	36.4(9)	15.2(9)	4.6(4)	3.3(5)
clinochlore	6.7(4)	18.4(5)	4.1(5)	15.8(4)	25.4(7)	23.8(8)	32.6(6)	22.6(7)	23.5(8)	12.4(5)	20.0(5)
dolomite	5.9(3)	5.8(2)	-	-	-	1.4(2)	-	-	0.4(4)	-	-
hematite	-	-	-	1.3(2)	1.2(2)	1.5(2)	1.7(2)	1.8(2)	2.6(3)	-	-
enstatite	-	-	-	1.2(3)	1.9(4)	3.1(6)	2.5(7)	1.4(4)	10.5(9)	8.3(5)	6.0(5)
forsterite	-	-	-	4.0(6)	3.2(7)	6.4(7)	5.7(4)	9.3(6)	6.0(7)	-	-
K-feldspar	-	-	-	-	-	-	-	-	-	5.6(5)	5.5(4)
magnetite	4.6(1)	3.5(1)	-	5.0(2)	5.4(2)	6.2(2)	6.9(2)	5.1(2)	-	-	-
muscovite/illite	6.8(7)	2.3(6)	15.0(5)	-	-	-	-	-	7.6(9)	13.9(9)	13.3(9)
plagioclase	3.7(4)	-	18.7(4)	-	-	-	-	-	8.3(4)	12.9(4)	11.3(4)
quartz	5.5(2)	1.9(1)	40.1(1)	-	-	-	-	-	6.3(2)	12.5(2)	10.4(2)
talc	-	1.3(3)	1.6(2)	-	-	4.6(9)	-	-	8.4(9)	9.6(4)	9.0(4)
tremolite	4.7(4)	-	4.0(3)	-	-	-	-	-	5.9(5)	11.2(3)	12.4(3)
TOT	100	100	100	100	100	100	100	100	100	100	100

Always consult and cite the final, published document. See http://www.minsocam.org or GeoscienceWorld

1146 **TABLE 5.** Summary of the calculated concentration of chrysotile asbestos in the

1147 four samples selected for the cross-check analysis.

Method	Normative reference	Chrysotile wt% STD1	Chrysotile wt% STD2	Chrysotile wt% C2	Chrysotile wt% E1
		Weighed value 5.11	Weighed value 10.44		
DTA	-	7.6	12.2	8.9	22.2
FTIR	Italian D.M. 09-06-94	4.9	13.8	6.3	32.9
PCOM	Italian D.M. 09-06-94	3.7	1.4	n.d.	7.5
SEM	Italian D.M. 09-06-94 - LAB1	4.6	13.1	4.7	27.5
SEM	Italian D.M. 09-06-94 - LAB2	1.9	0.6	5.9	26.4
XRPD external standard method	Italian D.M. 09-06-94	n.d.	n.d.	n.d.	n.d.
XRPD Rietveld method	-	5.8	11.2	6.3	25.3

1148

1149

Always consult and cite the final, published document. See http://www.minsocam.org or GeoscienceWorld

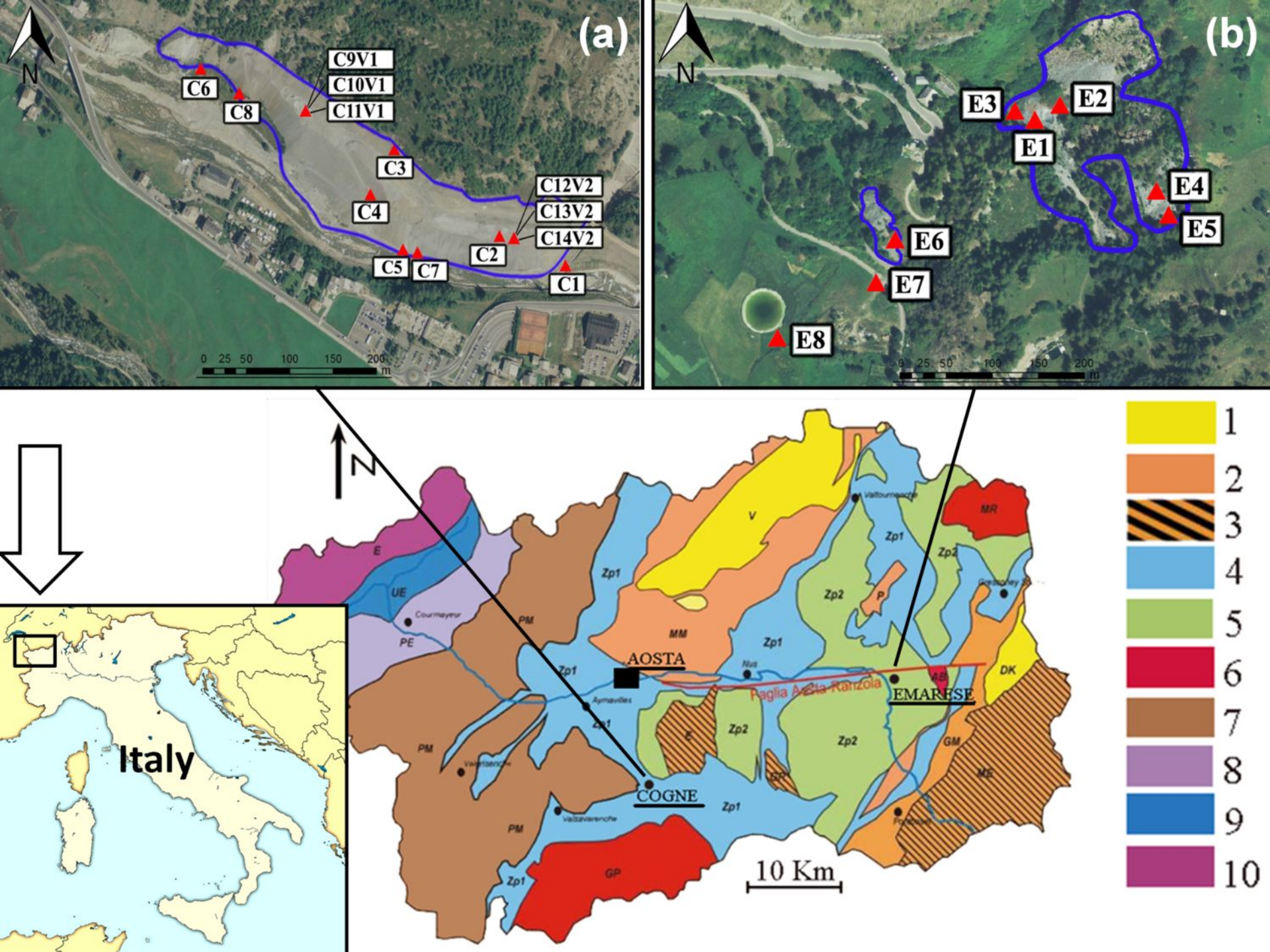
(a)
C6
C8
C9V1
C10V1
C11V1
C3
C4
C12V2
C13V2
C14V2
C2
C5
C7
C1
0 25 50 100 150 200 m
(b)
E3
E2
E1
E4
E5
E6
E7
E8
0 25 50 100 150 200 m
N
Italy
AOSTA
EMARESE
COGNE
Paglia Avella Ranzola
10 Km
1
2
3
4
5
6
7
8
9
10

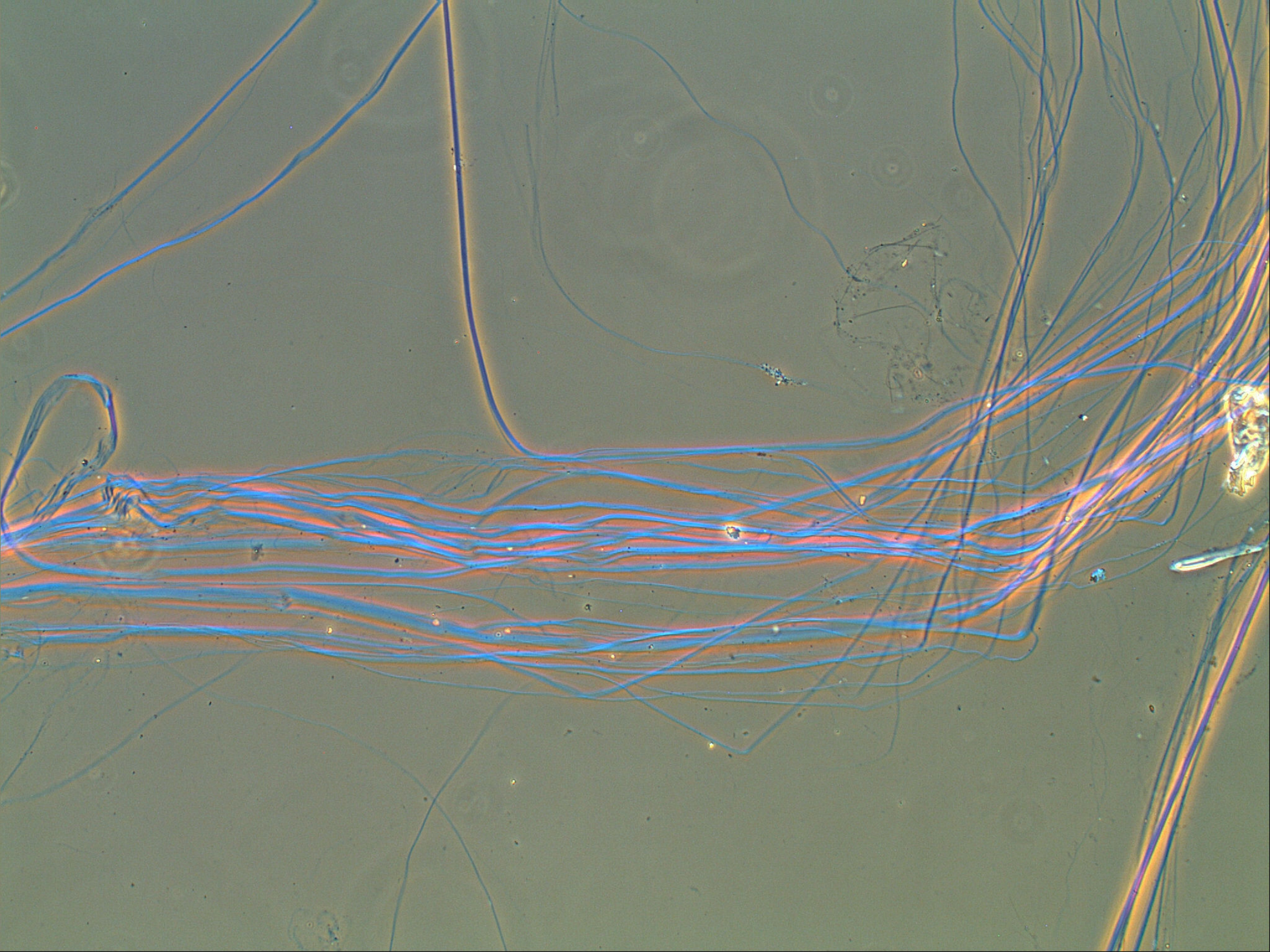

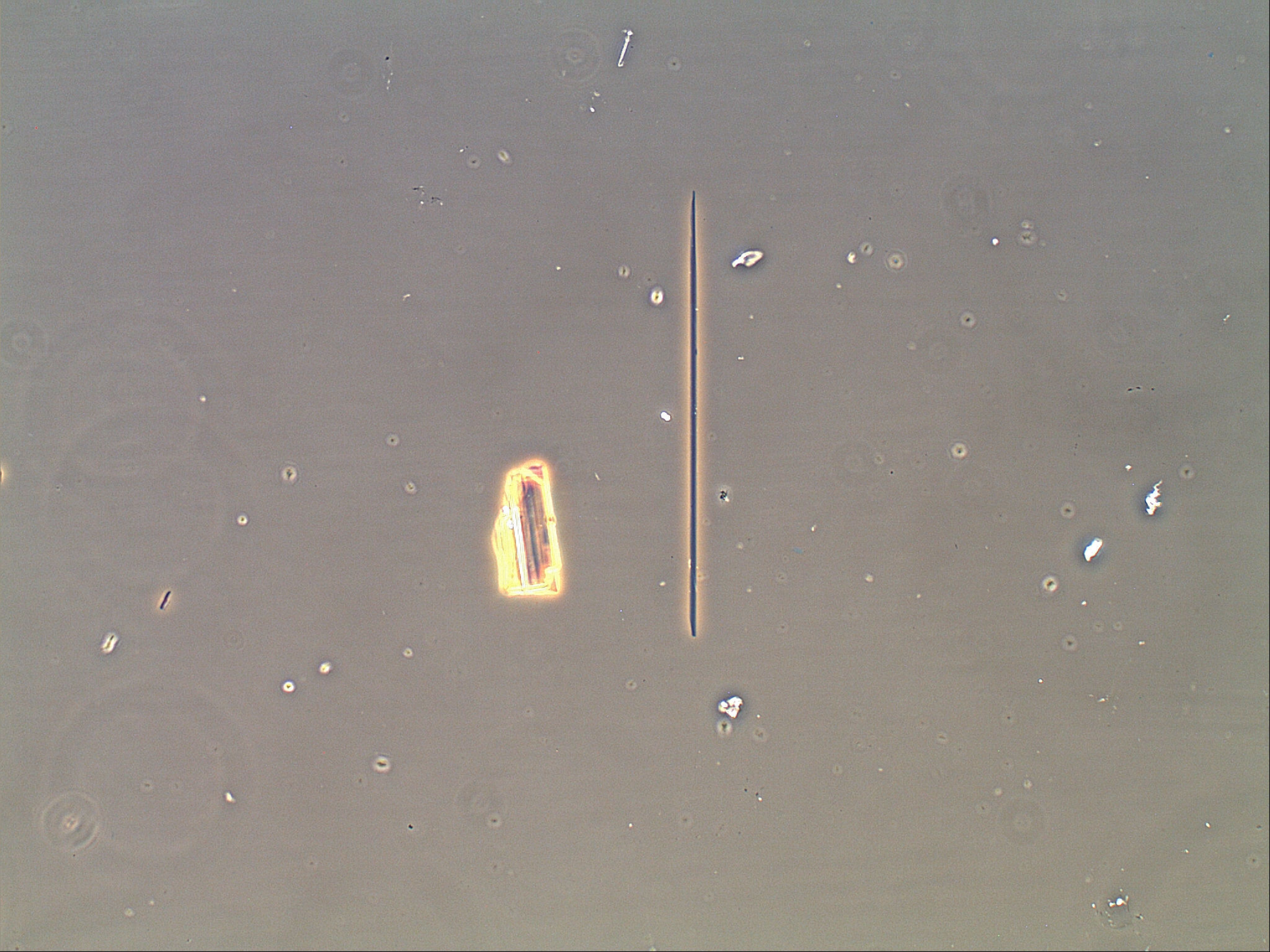

a
40 µm

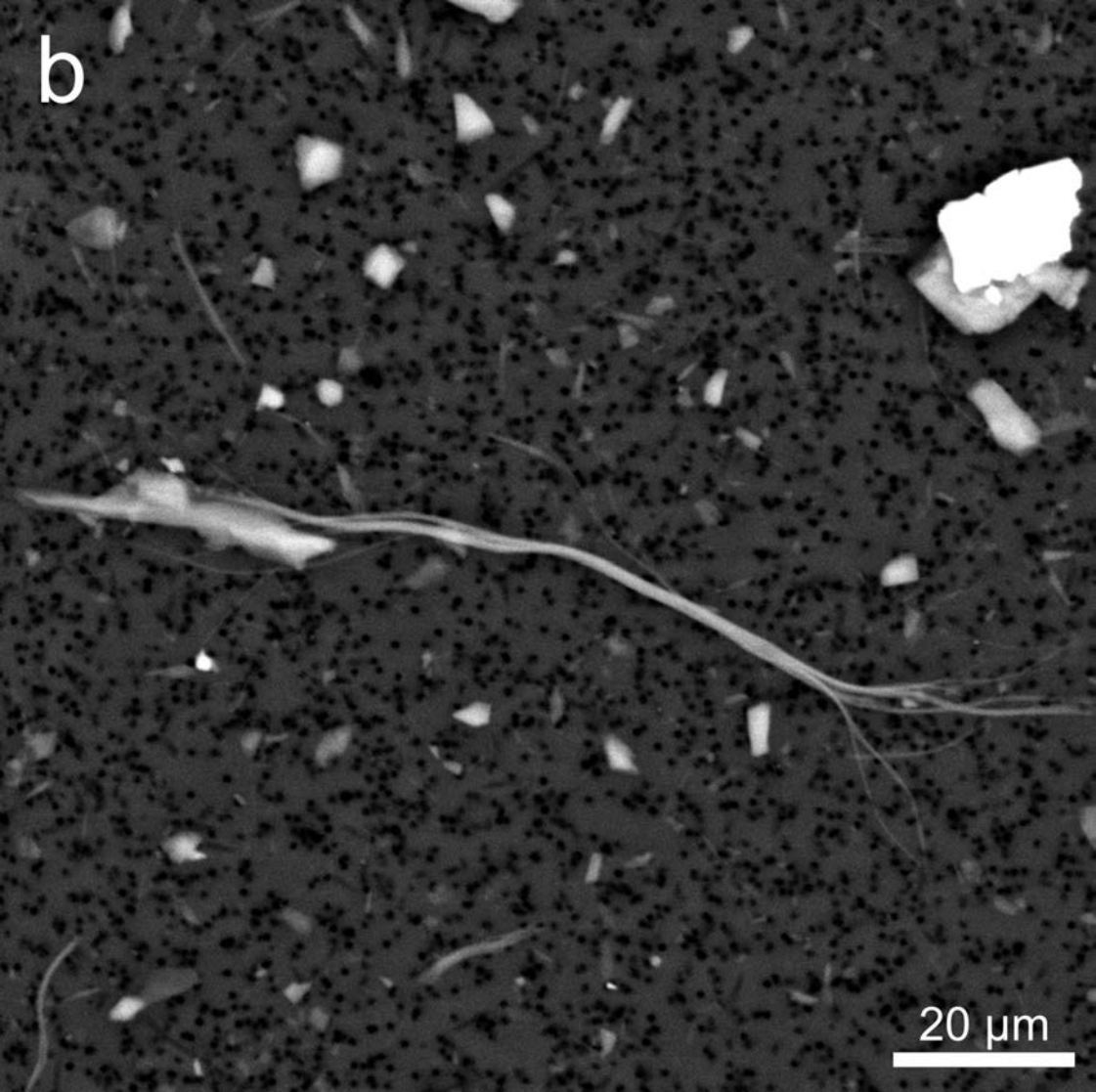
b
20 µm

C

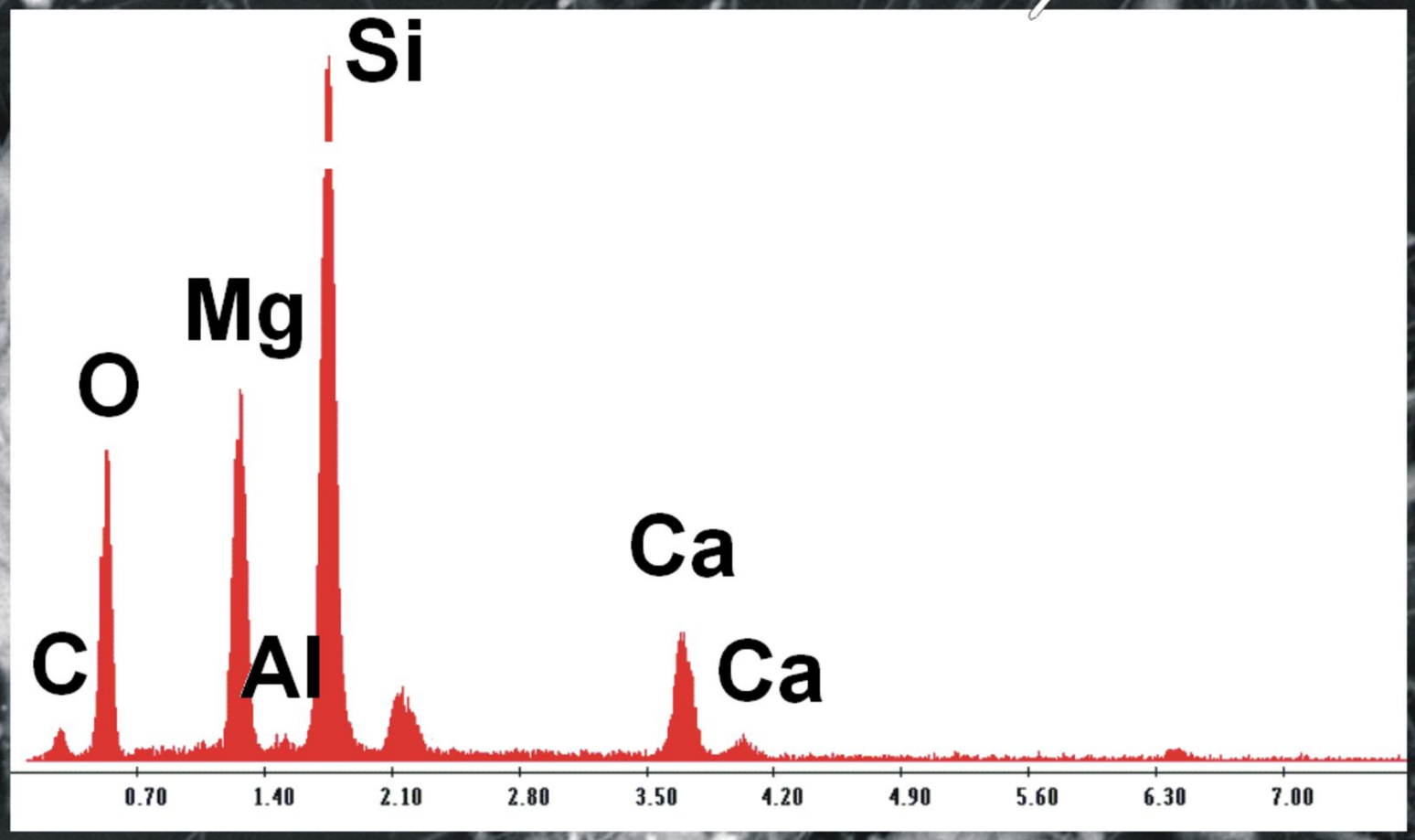

50 µm

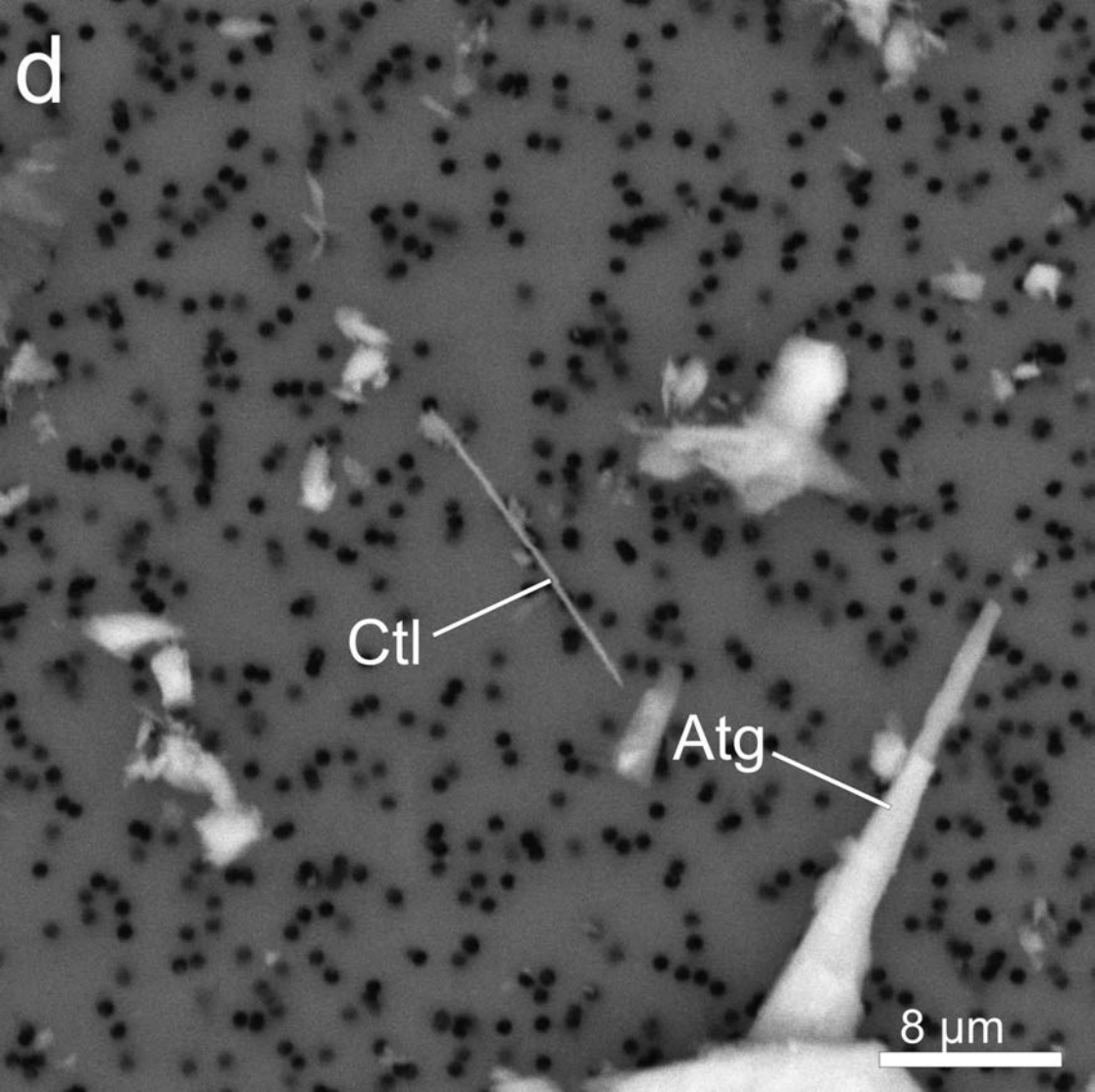
d
Ctl
Atg
8 µm

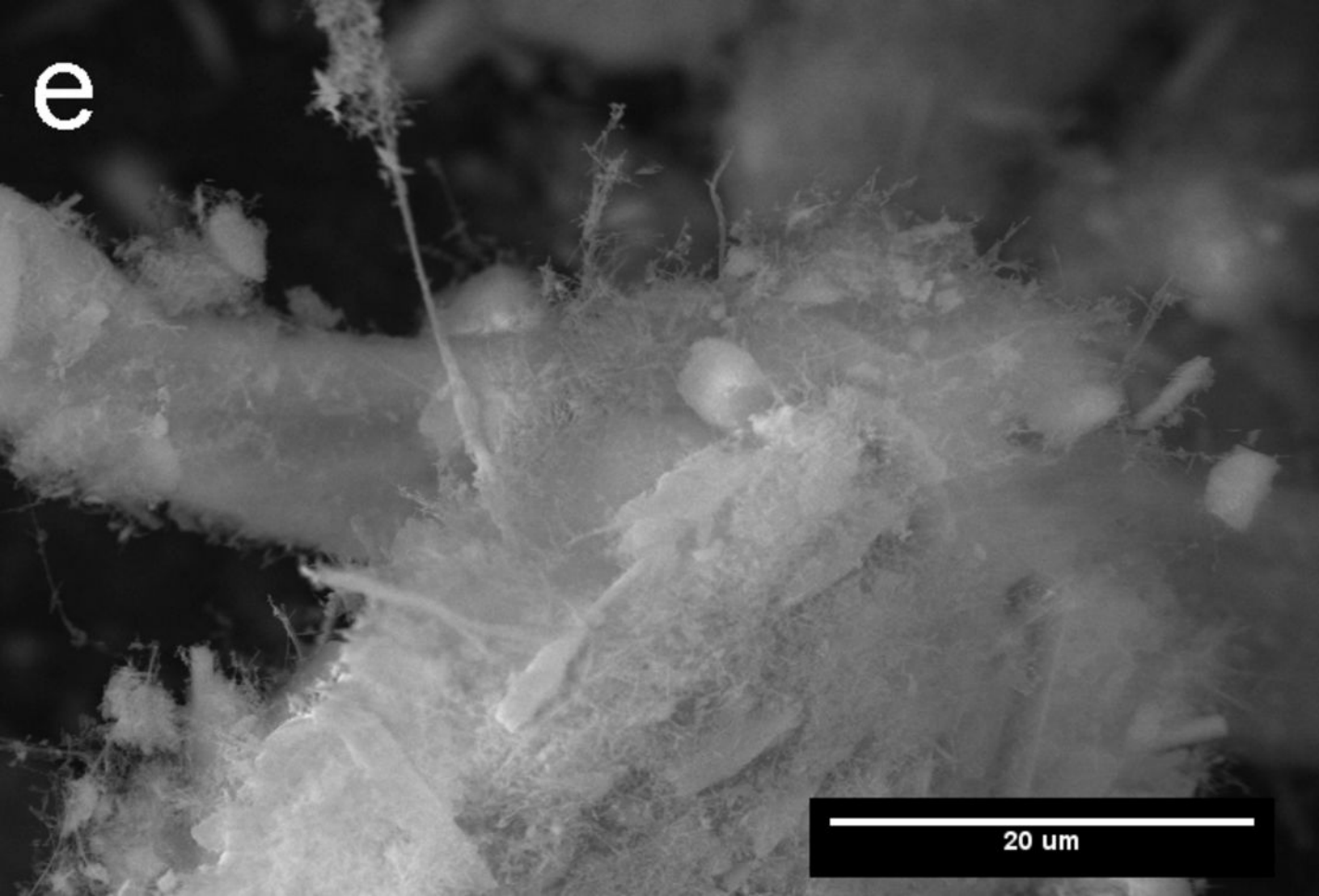
e
20 um

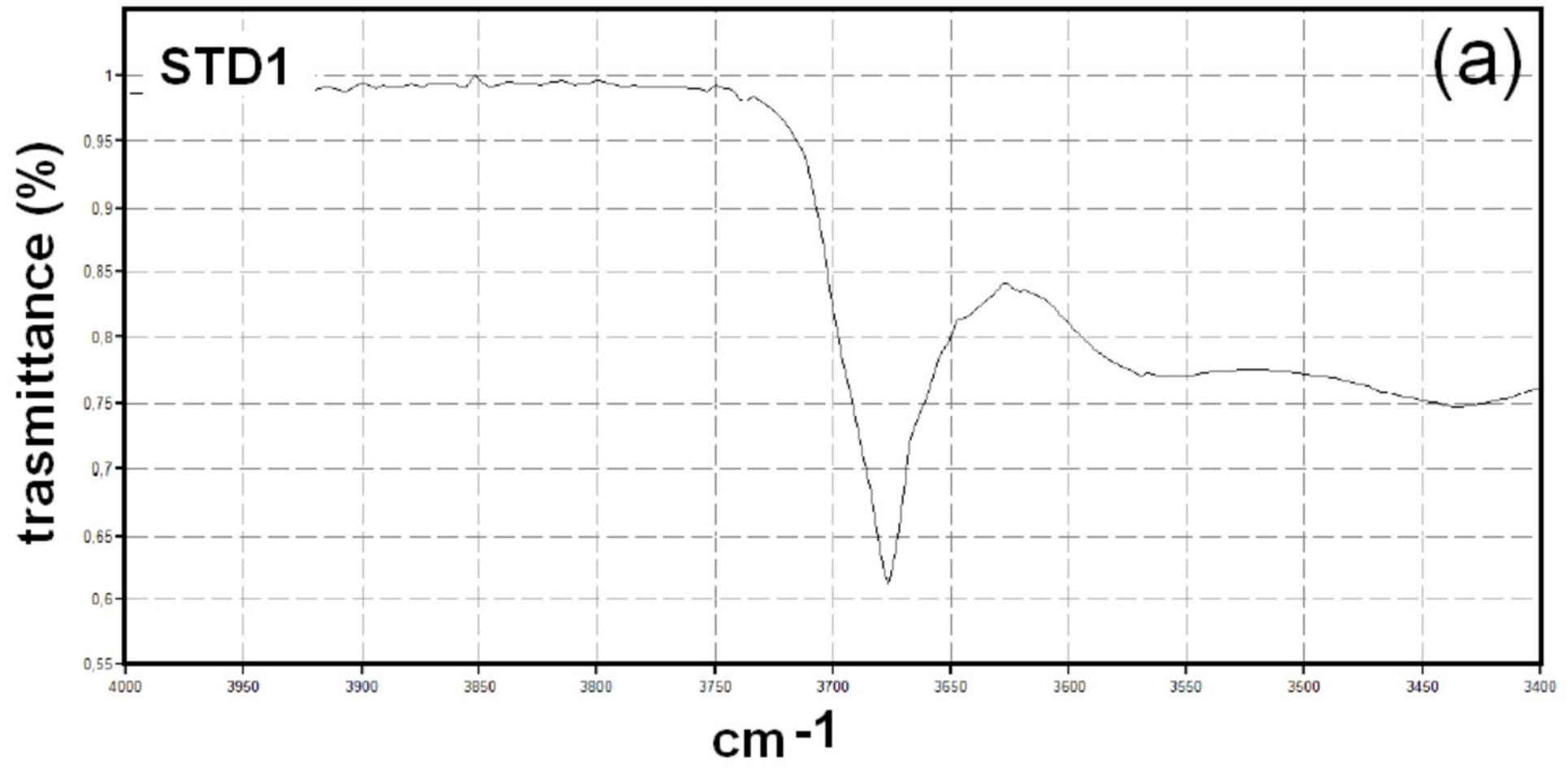
STD1
(a)
trasmittance (%)
1
0,95
0,9
0,85
0,8
0,75
0,7
0,65
0,6
0,55
4000
3950
3900
3850
3800
3750
3700
3650
3600
3550
3500
3450
3400
cm -1

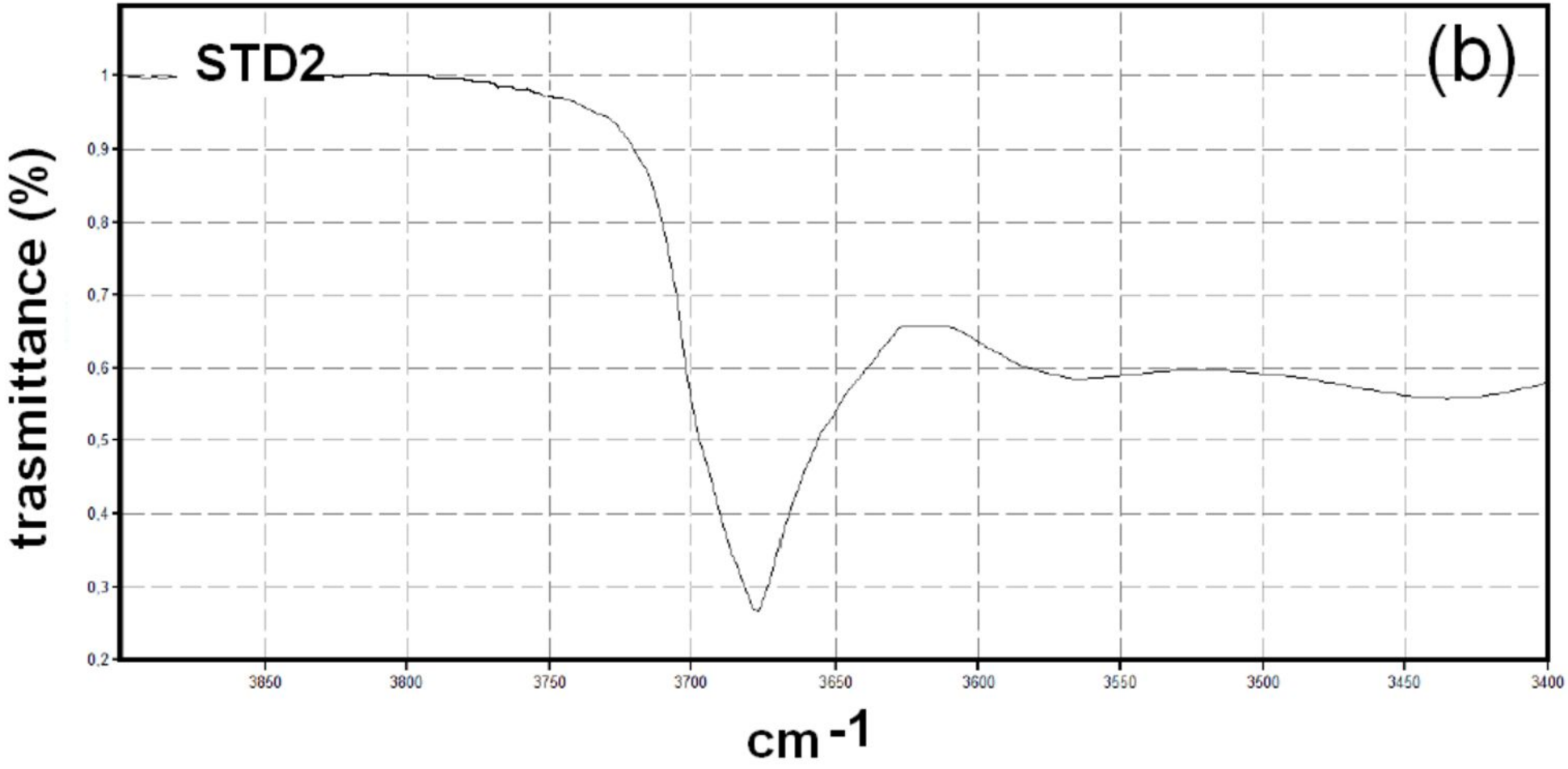
STD2
(b)
trasmittance (%)
1
0,9
0,8
0,7
0,6
0,5
0,4
0,3
0,2
3850
3800
3750
3700
3650
3600
3550
3500
3450
3400
cm -1

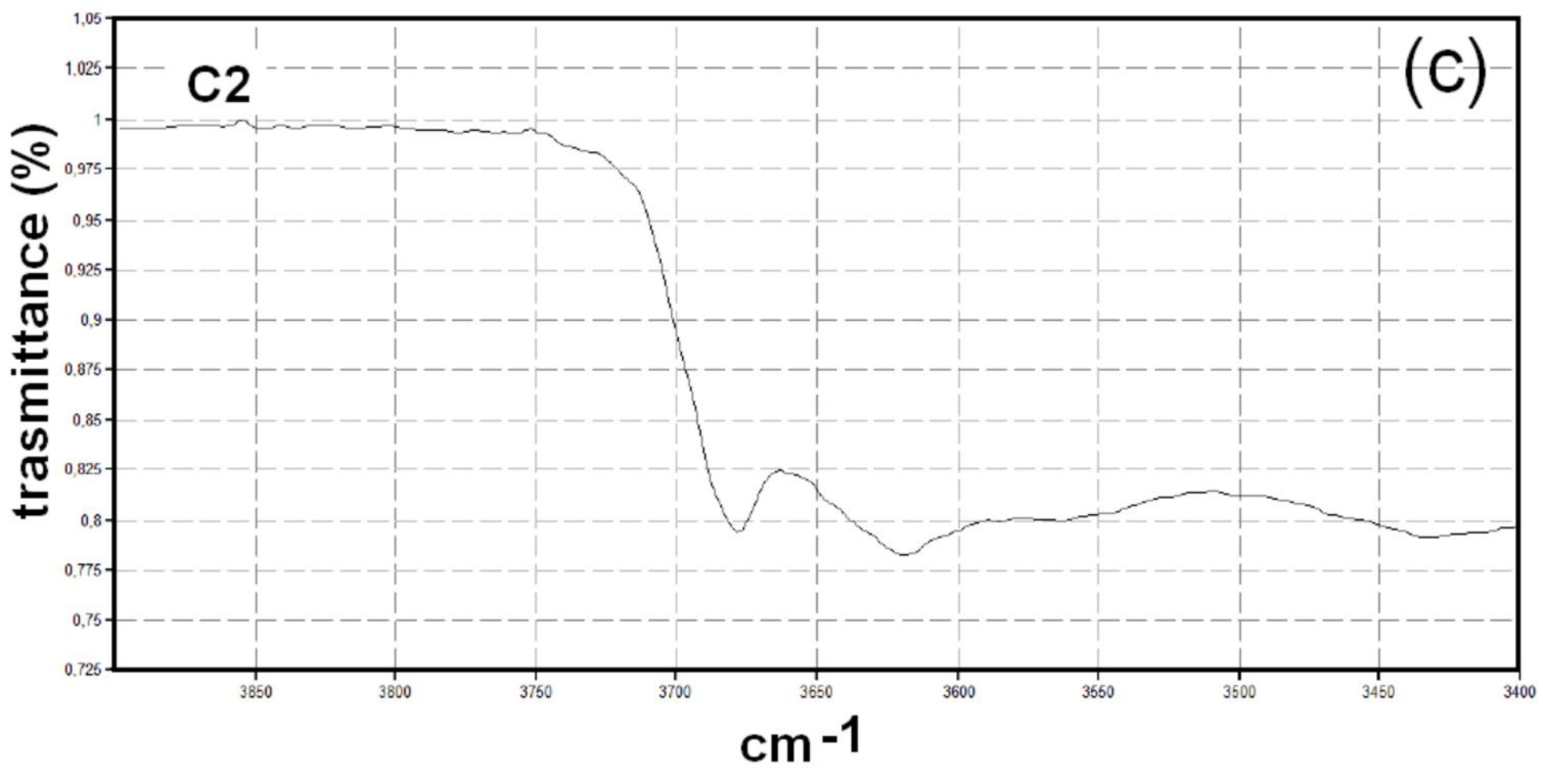
C2
(c)
trasmittance (%)
1,05
1,025
1
0,975
0,95
0,925
0,9
0,875
0,85
0,825
0,8
0,775
0,75
0,725
3850
3800
3750
3700
3650
3600
3550
3500
3450
3400
cm -1

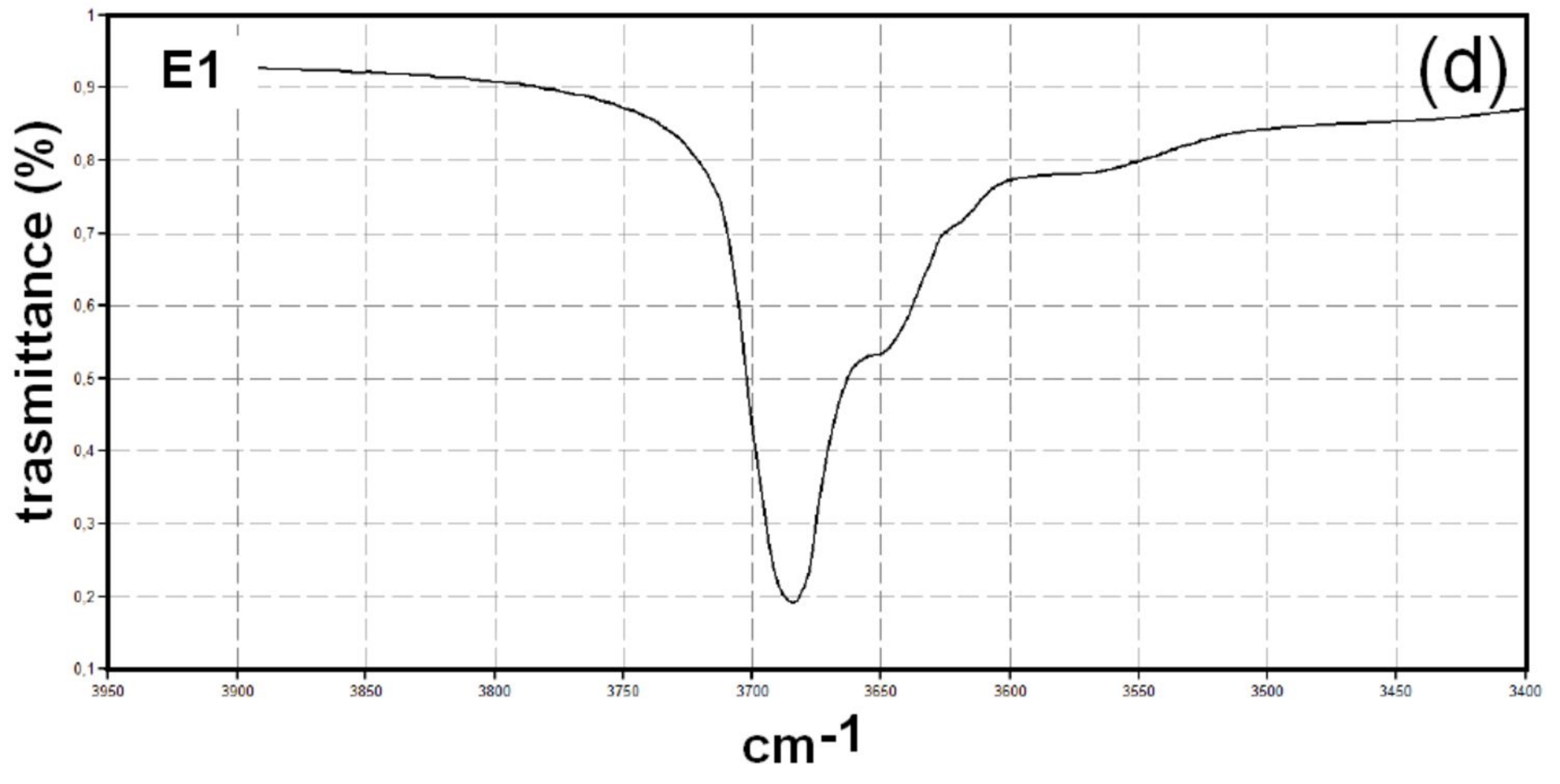
E1
(d)
trasmittance (%)
1
0,9
0,8
0,7
0,6
0,5
0,4
0,3
0,2
0,1
3950
3900
3850
3800
3750
3700
3650
3600
3550
3500
3450
3400
cm-1

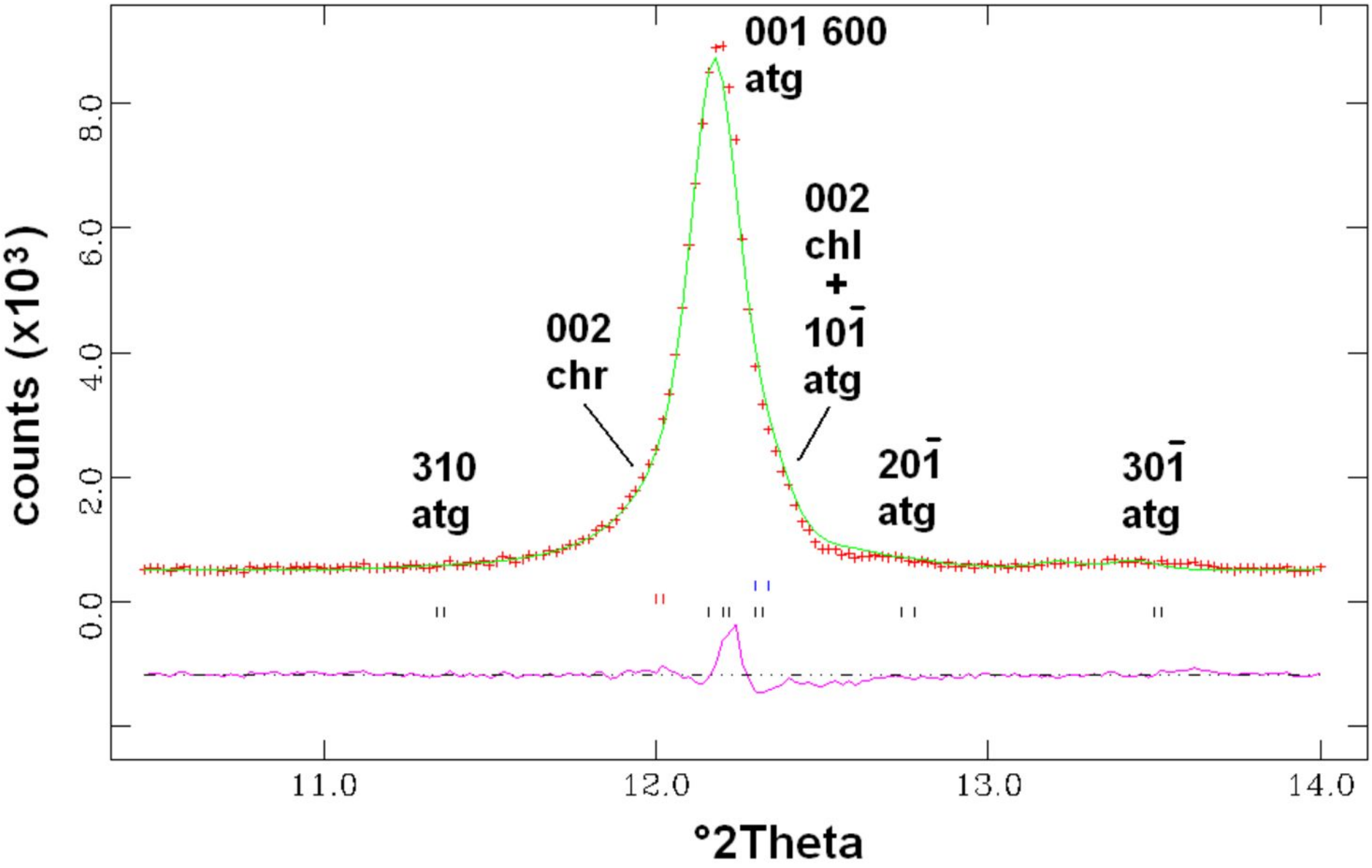
001 600
atg
002
chl
+
10$\bar{1}$
atg
002
chr
310
atg
20$\bar{1}$
atg
30$\bar{1}$
atg
counts (x10³)
0.0
2.0
4.0
6.0
8.0
11.0
12.0
13.0
14.0
°2Theta

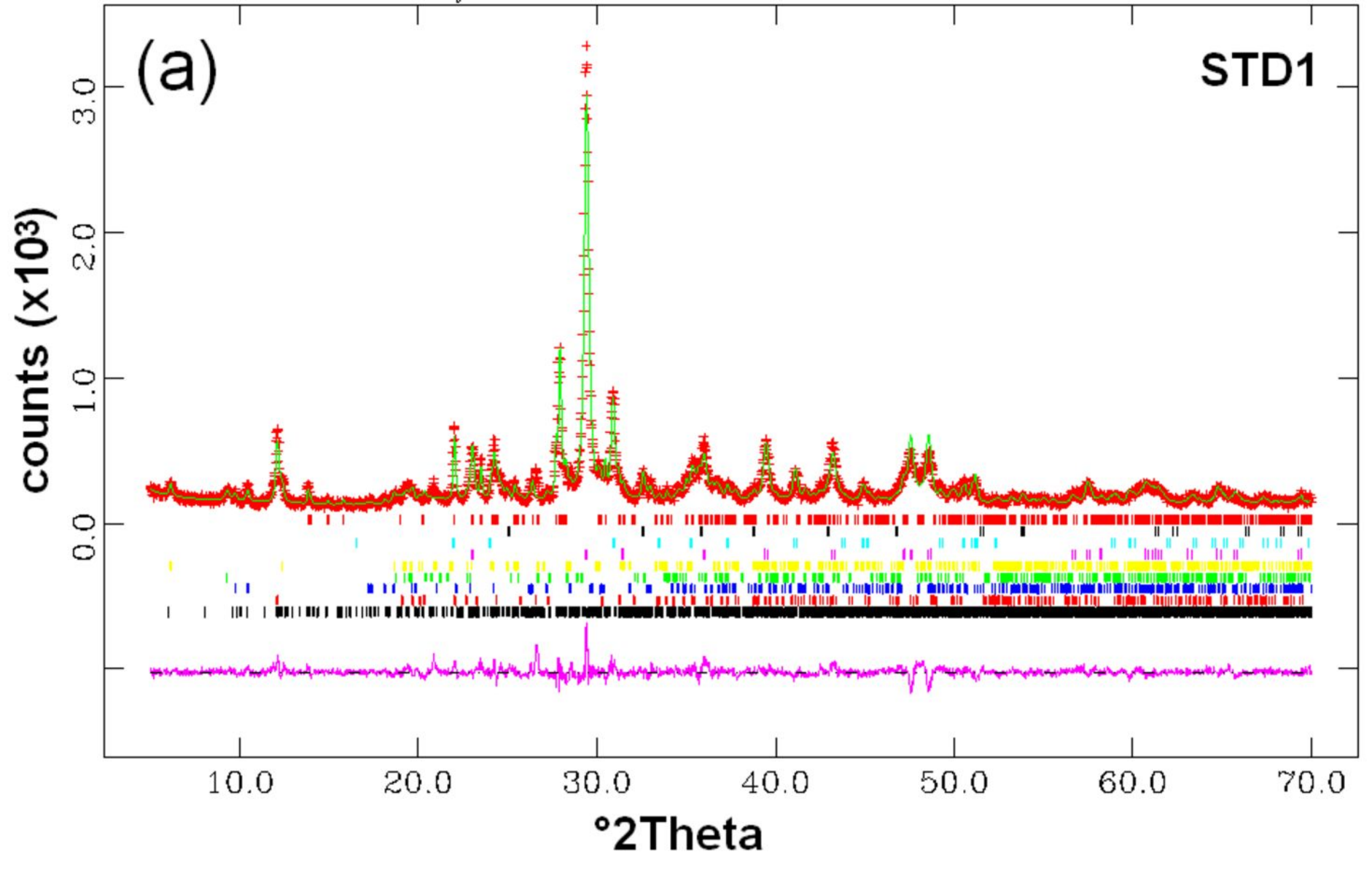
(a)
STD1
counts (x10³)
3.0
2.0
1.0
0.0
10.0
20.0
30.0
40.0
50.0
60.0
70.0
°2Theta

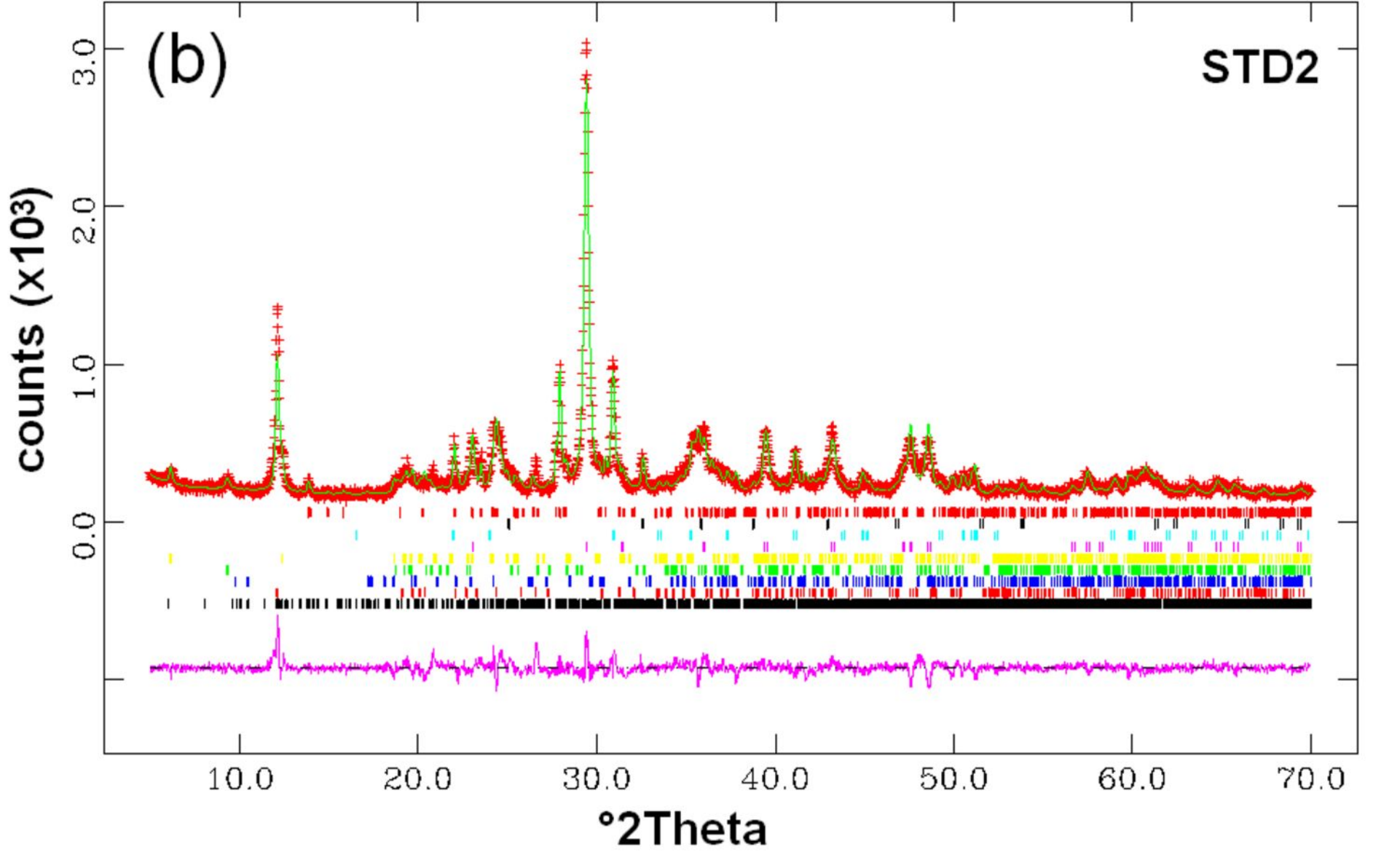
(b)
STD2
counts (x10³)
3.0
2.0
1.0
0.0
10.0
20.0
30.0
40.0
50.0
60.0
70.0
°2Theta

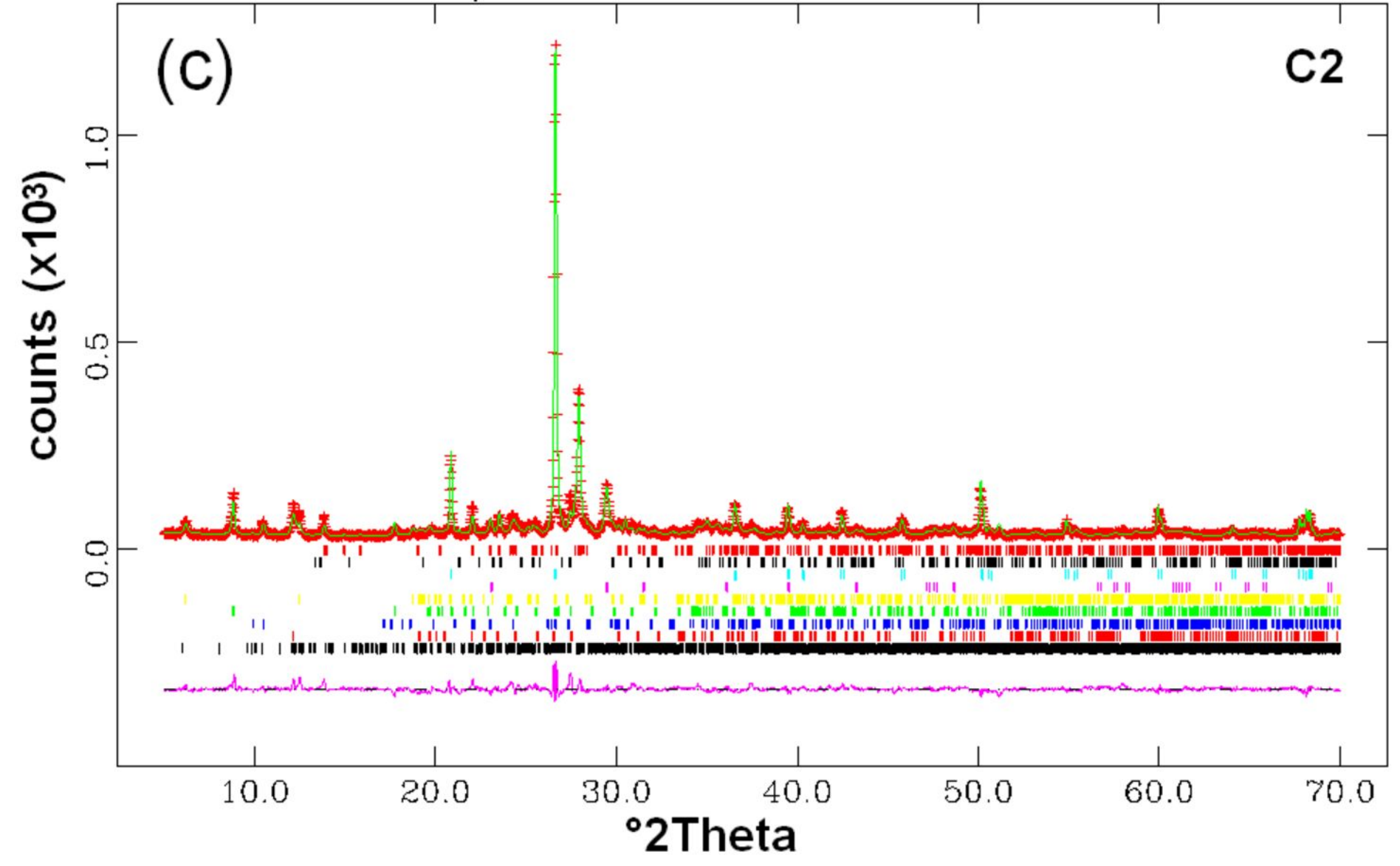
(c)
C2
counts (x10³)
1.0
0.5
0.0
10.0
20.0
30.0
40.0
50.0
60.0
70.0
°2Theta

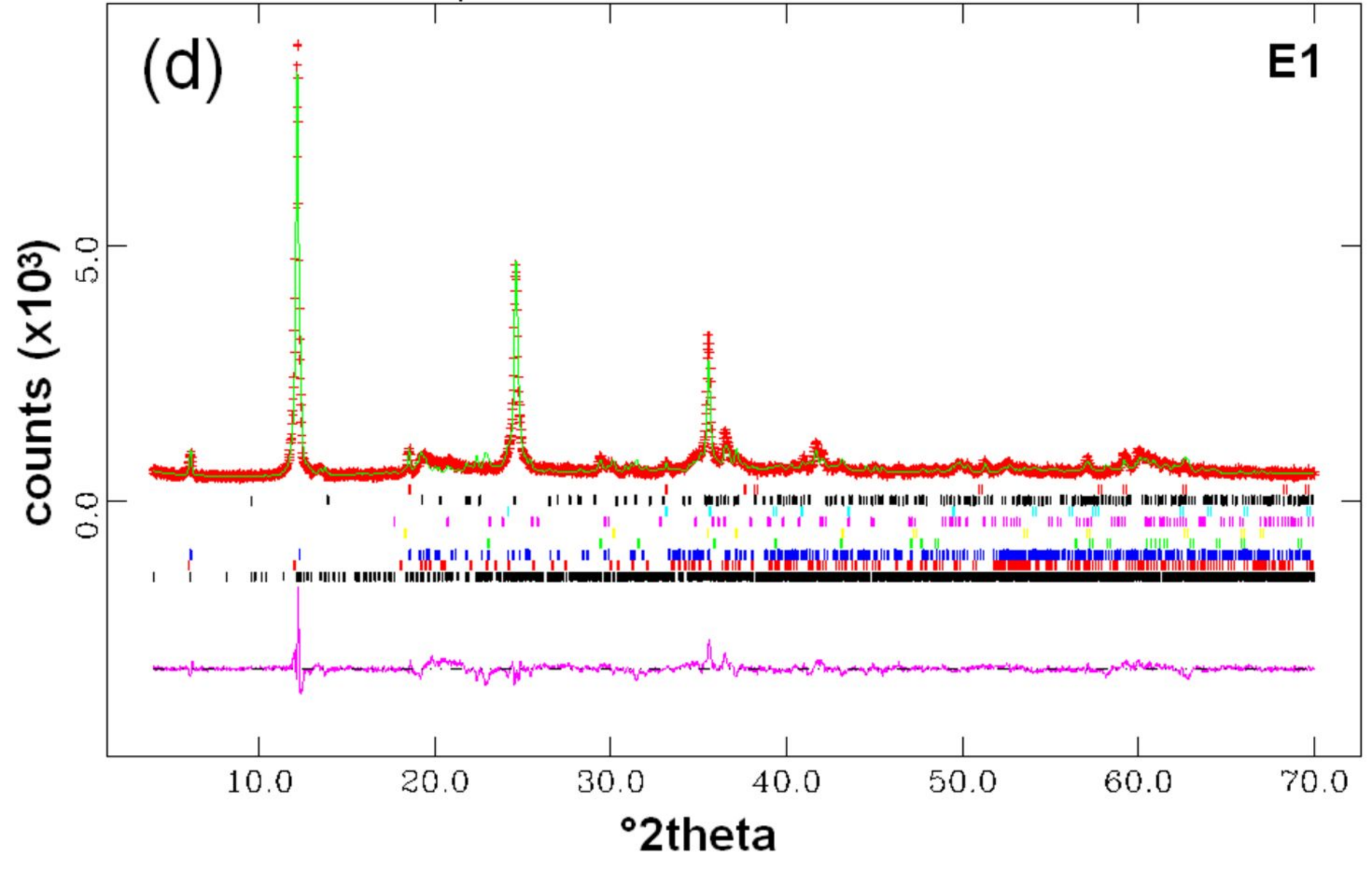
(d)
E1
counts (x10³)
5.0
0.0
10.0
20.0
30.0
40.0
50.0
60.0
70.0
°2theta

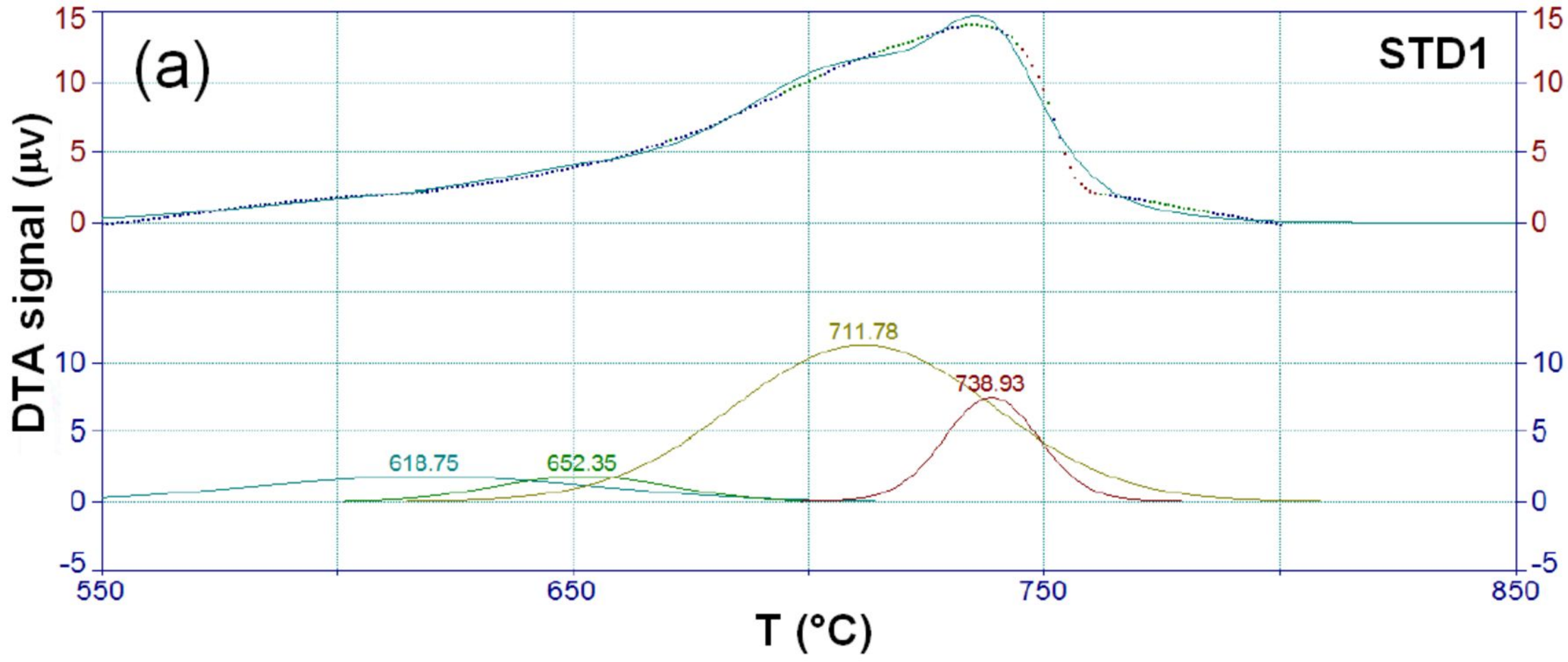
(a)
STD1
DTA signal (µv)
15
10
5
0
-5
711.78
738.93
618.75
652.35
550
650
750
850
T (°C)

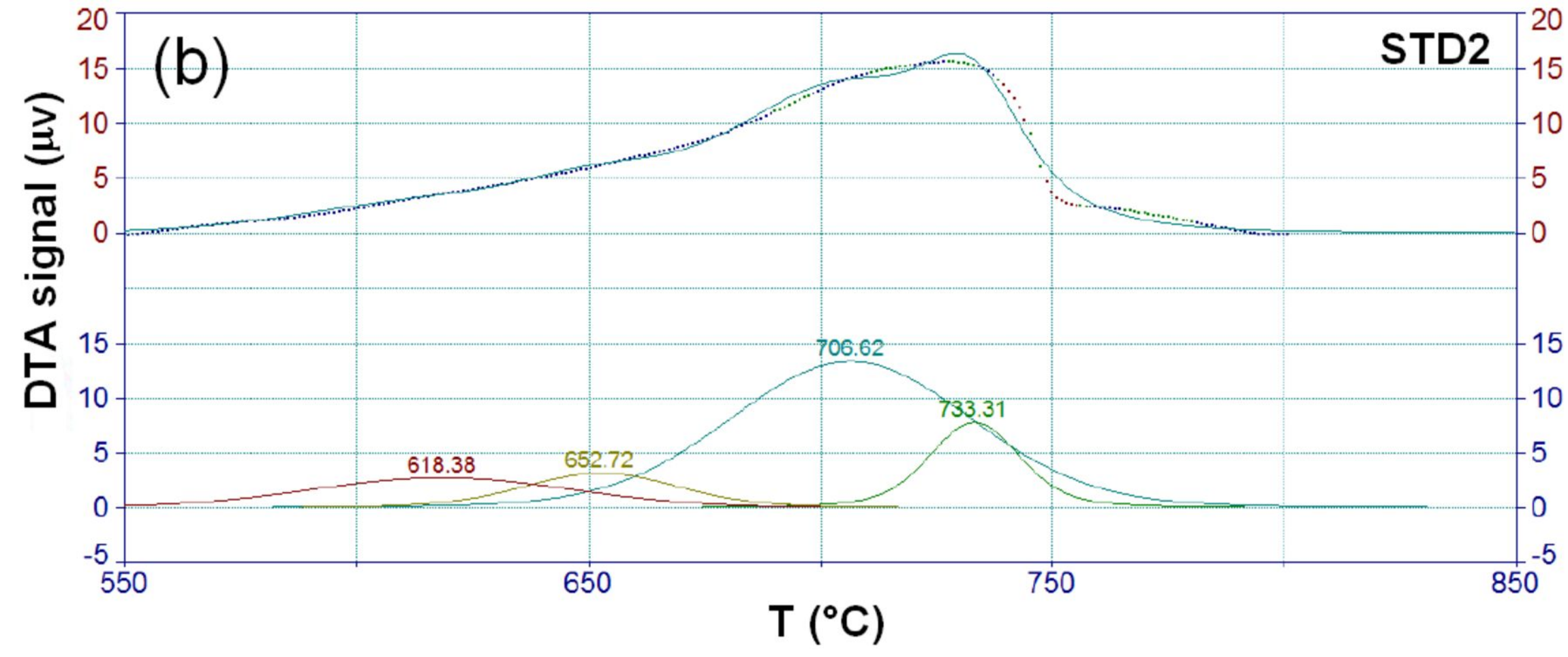
(b)
STD2
DTA signal (µv)
20
15
10
5
0
-5
706.62
733.31
618.38
652.72
550
650
750
850
T (°C)

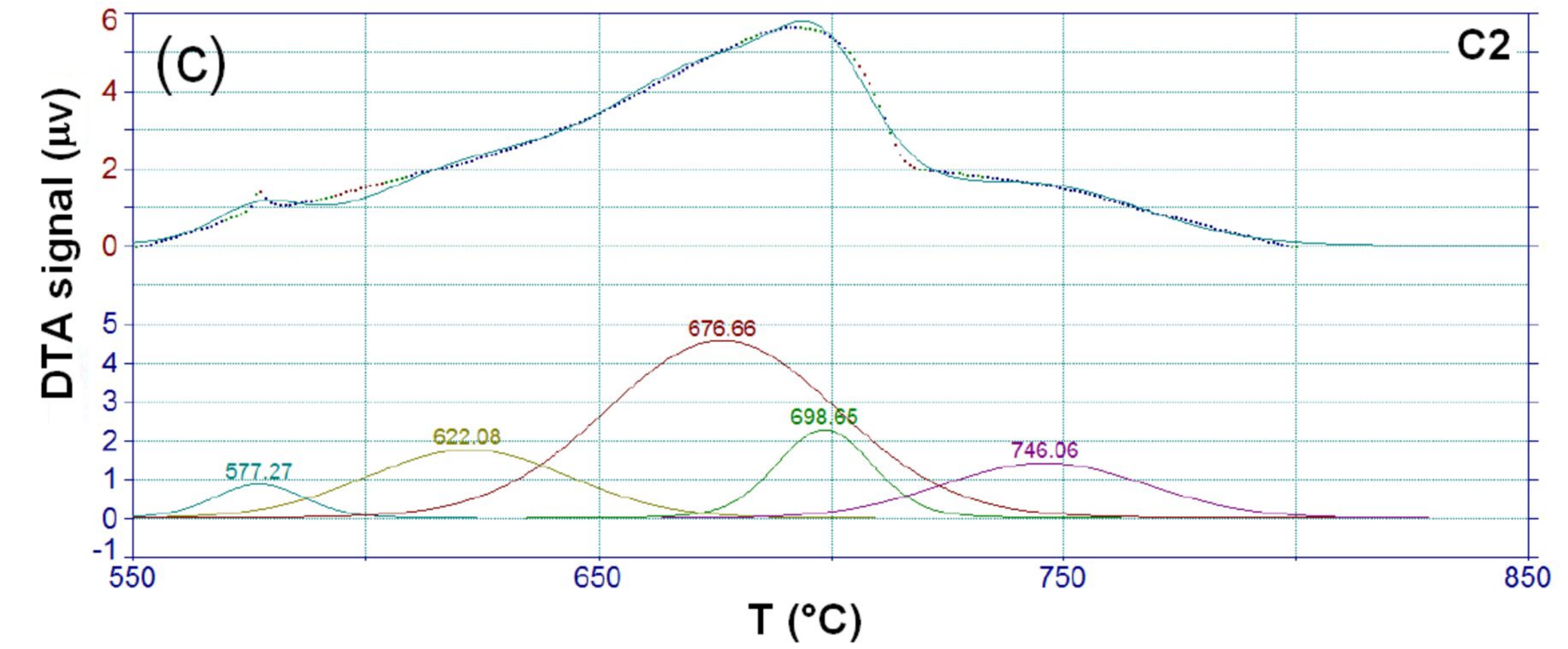
(C)
C2
DTA signal (µv)
6
4
2
0
5
4
3
2
1
0
-1
676.66
622.08
698.65
746.06
577.27
550
650
750
850
T (°C)

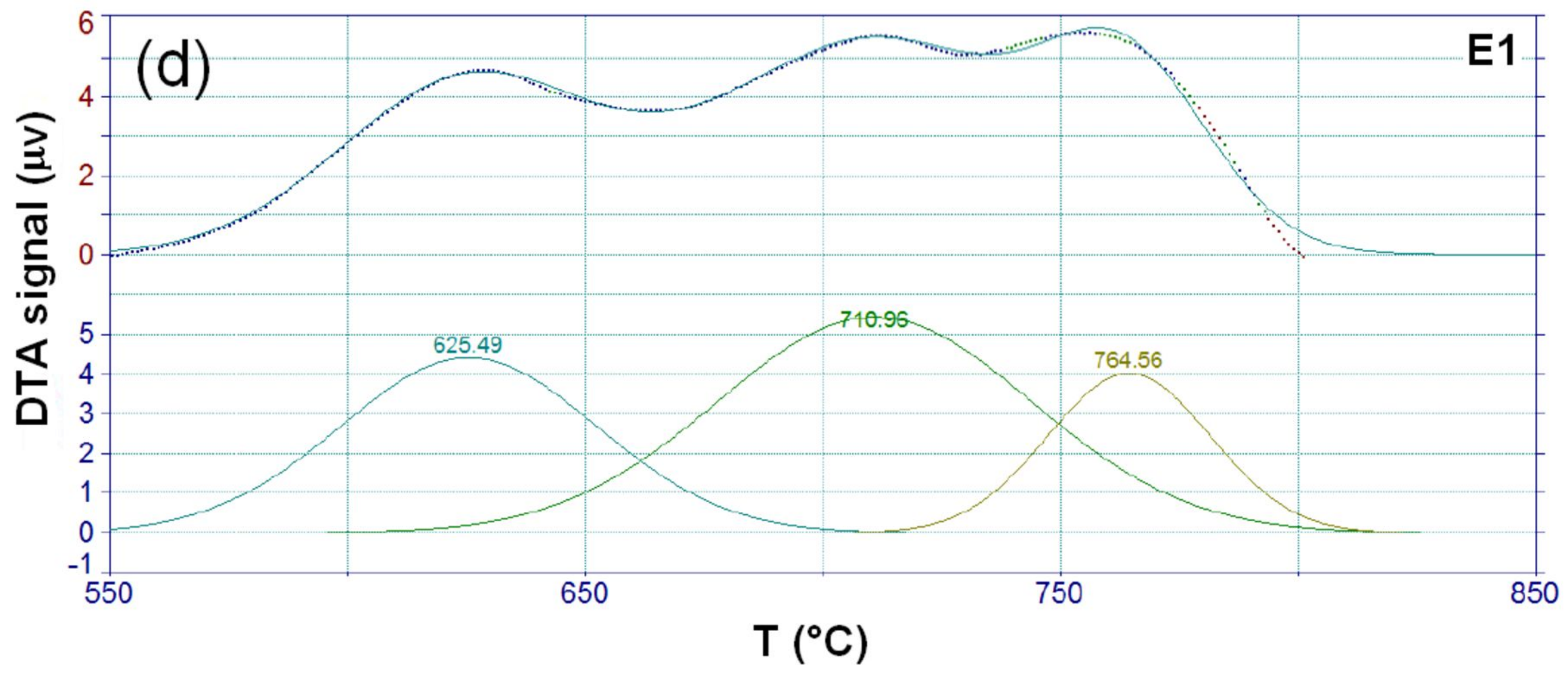
(d)
E1
DTA signal (µv)
6
4
2
0
5
4
3
2
1
0
-1
625.49
710.96
764.56
550
650
750
850
T (°C)

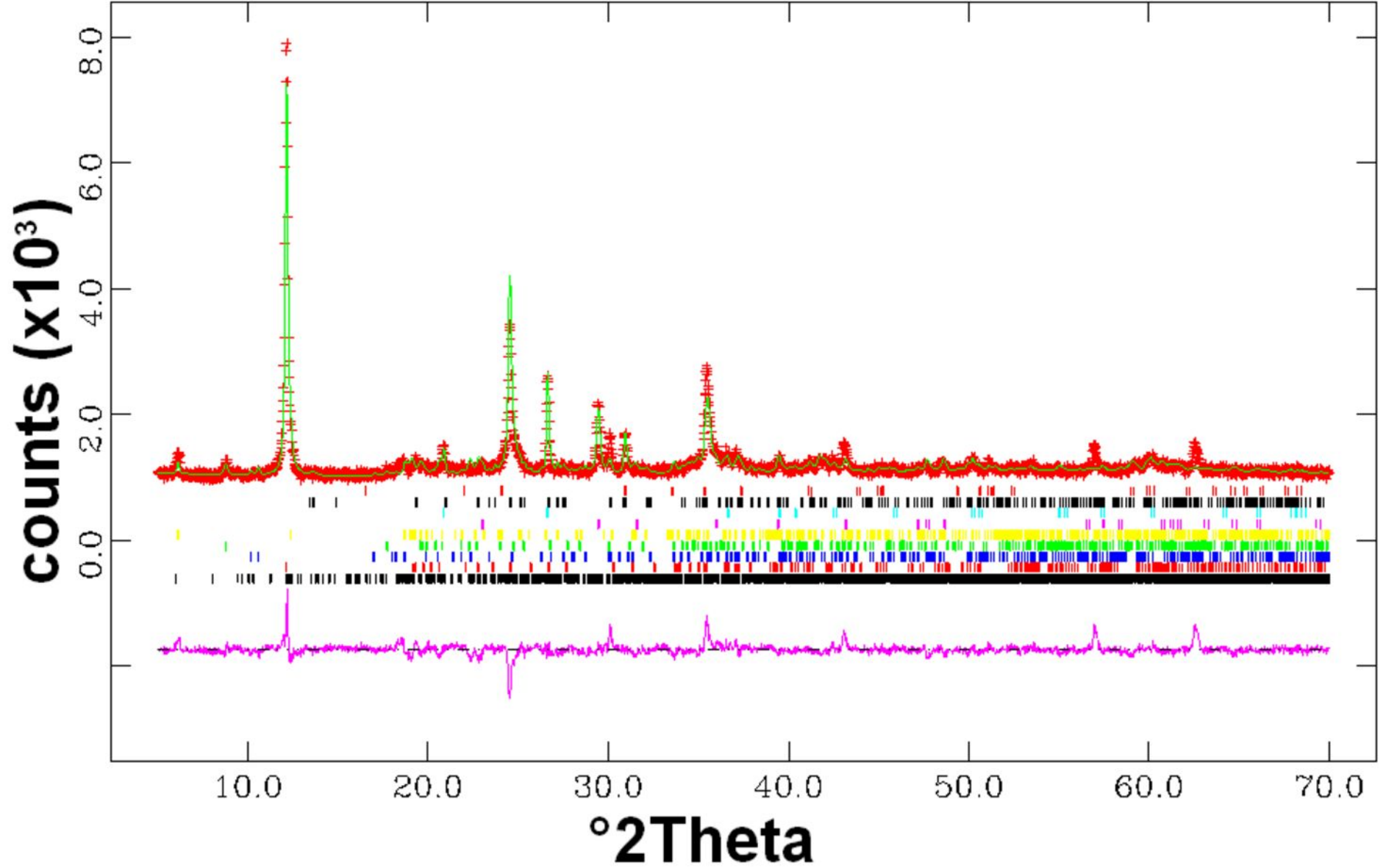
counts (x10³)
8.0
6.0
4.0
2.0
0.0
10.0
20.0
30.0
40.0
50.0
60.0
70.0
°2Theta

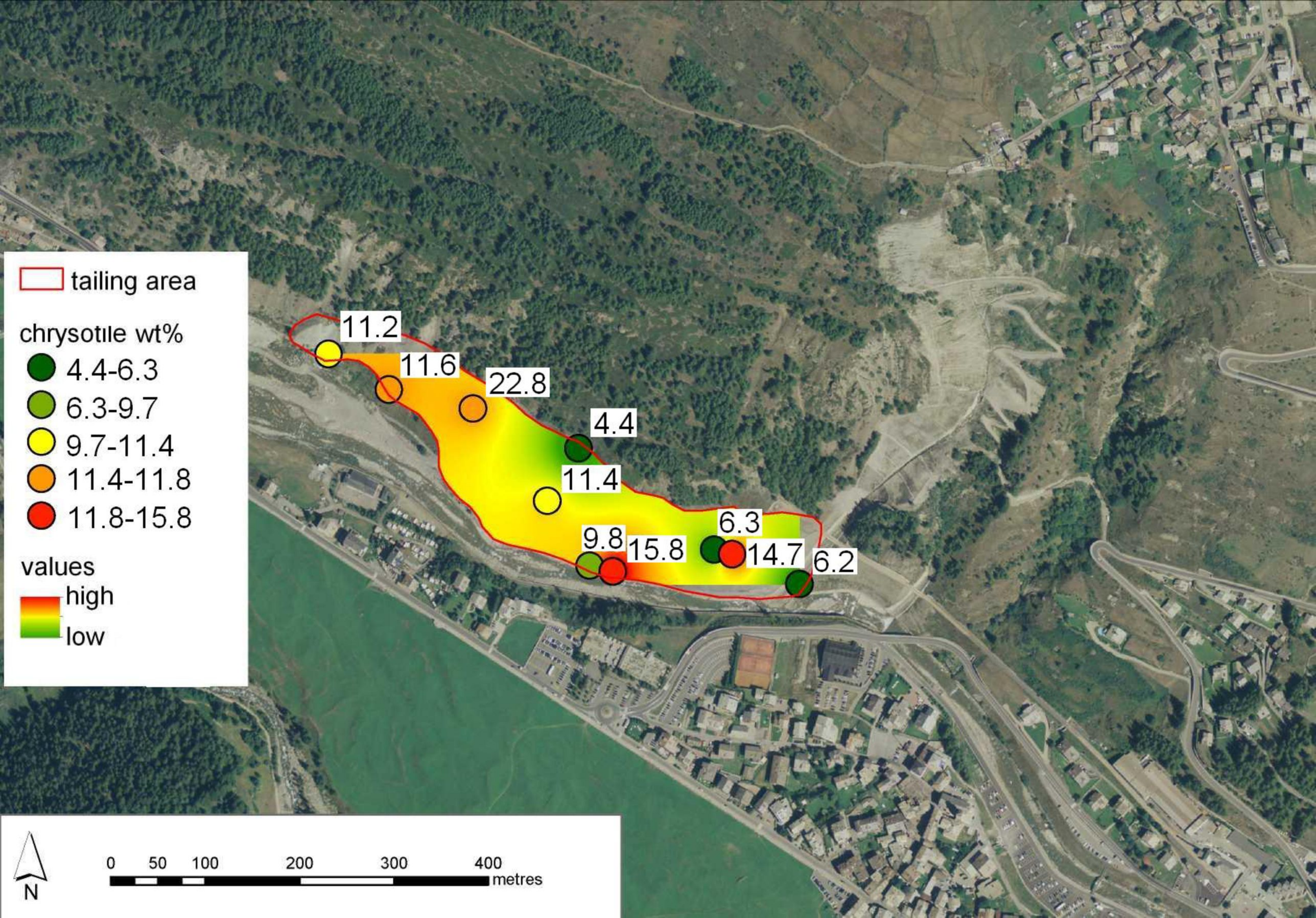
tailing area
chrysotile wt%
4.4-6.3
6.3-9.7
9.7-11.4
11.4-11.8
11.8-15.8
values
high
low
11.2
11.6
22.8
4.4
11.4
9.8
15.8
6.3
14.7
6.2
N
0
50
100
200
300
400
metres

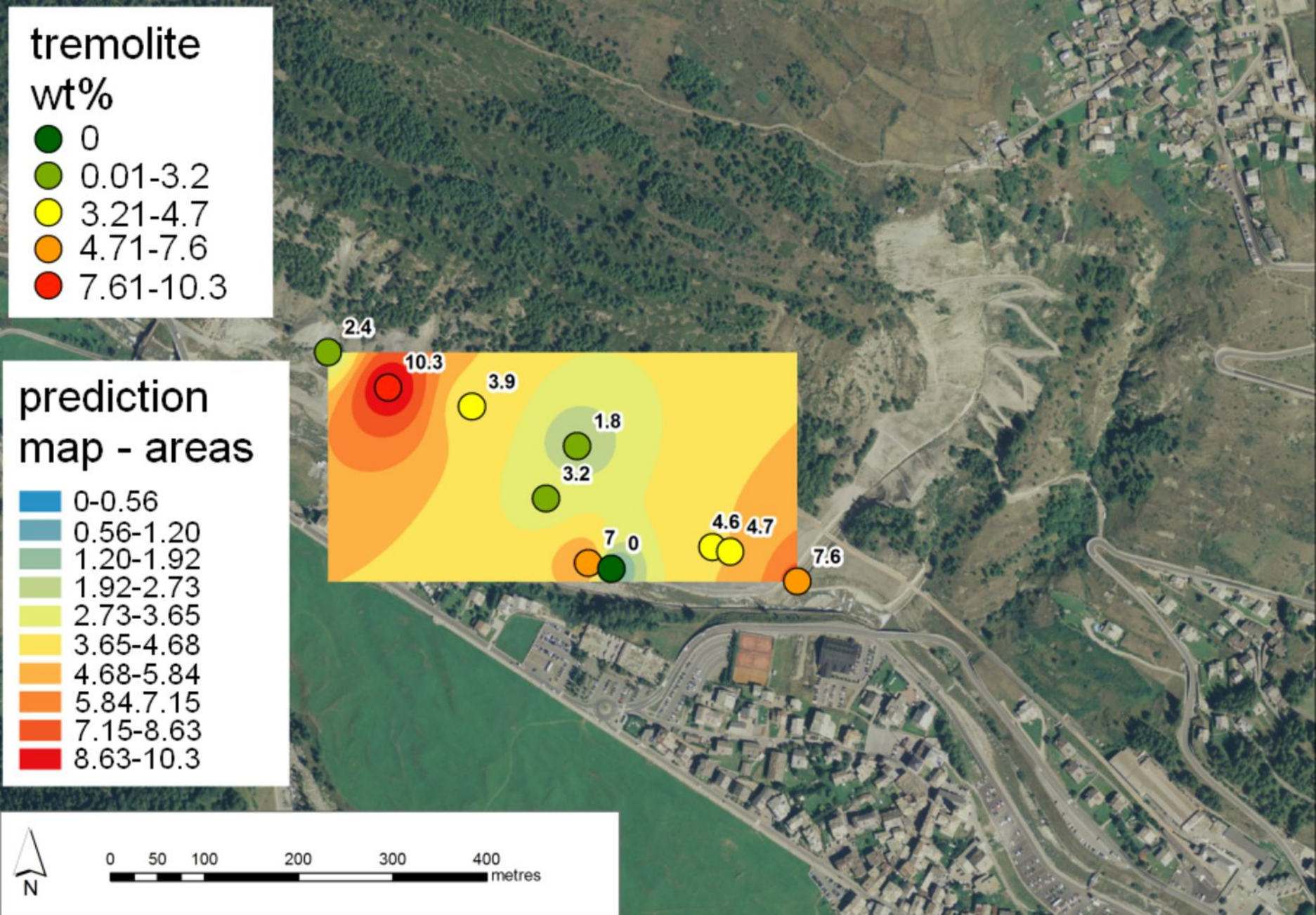
tremolite
wt%
0
0.01-3.2
3.21-4.7
4.71-7.6
7.61-10.3
prediction
map - areas
0-0.56
0.56-1.20
1.20-1.92
1.92-2.73
2.73-3.65
3.65-4.68
4.68-5.84
5.84.7.15
7.15-8.63
8.63-10.3
2.4
10.3
3.9
1.8
3.2
7
0
4.6
4.7
7.6
N
0
50
100
200
300
400
metres

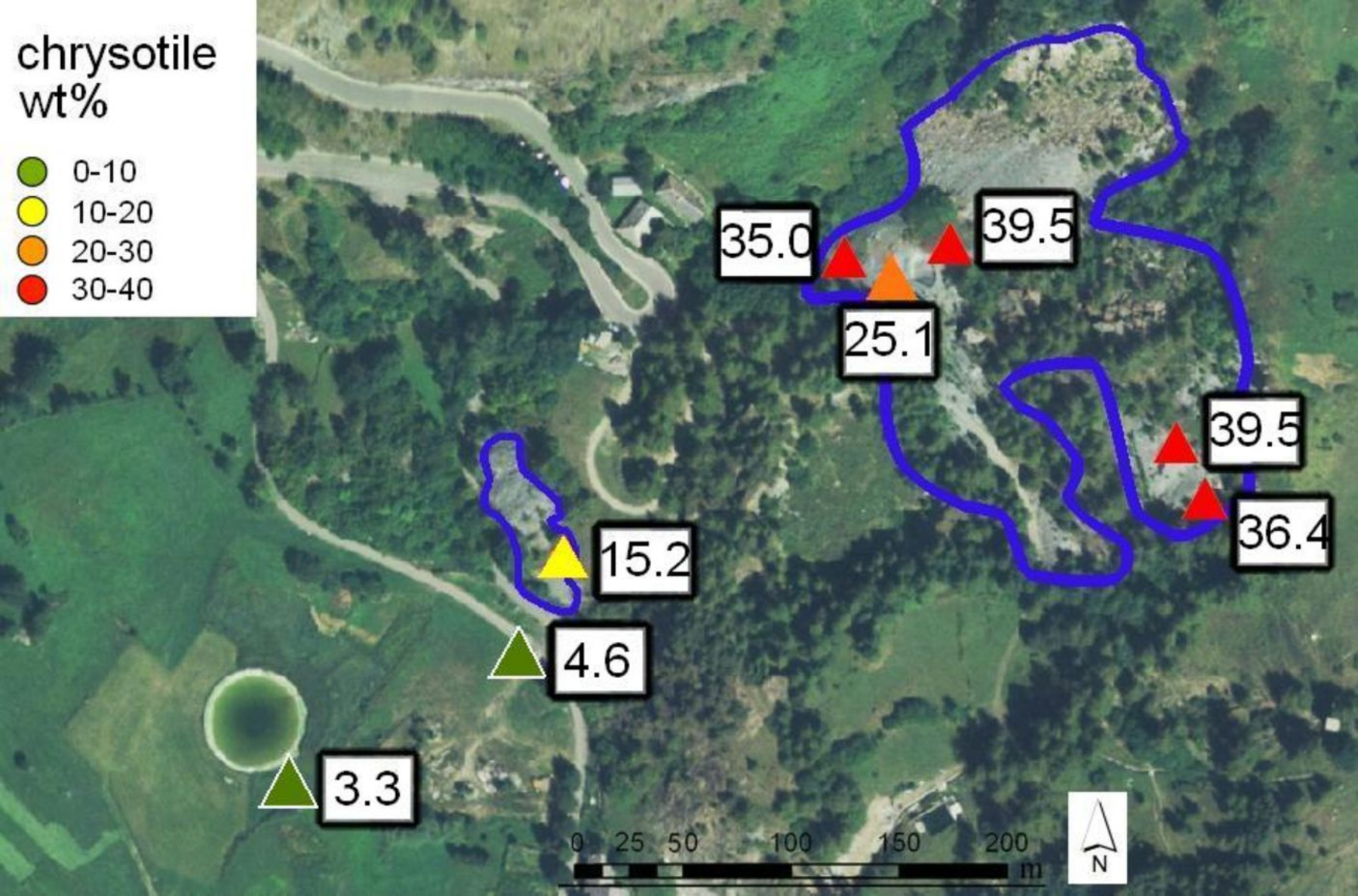
chrysotile
wt%
0-10
10-20
20-30
30-40
35.0
39.5
25.1
39.5
36.4
15.2
4.6
3.3
0
25
50
100
150
200
m
N